Table 1: Satellite Mass Budget (kg)

Radio astronomy payload	27.1
K_u-band communication	31.8
Deployable antenna	247.1
GPS receiver	7.8
Electric power	118.0
S-band communication	8.4
Command and data processing	15.8
Attitude and orbit control	78.4
Reaction control system (RCS)	30.0
Launch operation	6.4
Thermal control	20.0
Structure	117.6
Wire harness and others	45.0
Satellite dry mass	753.4
RCS propellant	62.0
Total mass	815.4

Table 2: Satellite Power Budget (W)

	Apogee	Perigee
Science payload	70.7	70.7
K_u communication system	44.3	44.3
K_u antenna	40.0	40.0
Solar panels	2.9	2.9
Power	4.8	4.8
S-band receiver	7.6	7.6
S-band transmitter	12.7	4.6
Command and data handling	15.6	15.6
Inertial reference units	37.3	37.3
Star trackers	69.4	69.4
Reaction wheels	26.4	26.4
Attitude control	10.6	10.6
Momentum unloading	0.0	18.2
GPS	9.7	31.4
Battery heater	29.2	29.2
Reaction control system heater	60.6	60.6
Sum	441.8	473.6
Conversion and other losses	92.5	100.4
Charging	30.2	30.2
Total power consumption	564.5	604.2

Table 3: Antenna Characteristics

Frequency (GHz)	1.66	4.85	22.15	Remarks
Gain (if 100% efficient) (dB)	42.86	52.17	65.36	Aperture area 50.1 m^2
Aperture illumination (dB)	−0.74	−0.90	−0.98	
Spillover (dB)	−2.44	−0.85	−0.40	
Blockage (dB)	−0.30	−0.30	−0.30	Subreflector supports
Surface accuracy (dB)	−0.01	−0.04	−0.94	0.5 mm RMS
Mesh reflectivity (dB)	−0.01	−0.01	−0.06	Mesh reflection loss
Dielectric loss (dB)	−0.01	−0.01	−0.08	White paint
Feed loss (dB)	−0.72	−0.55	−0.53	Horn, feed
Antenna gain (dB)	38.63	49.51	62.07	
Aperture efficiency (%)	38	54	47	

3 Science Subsystem of the VSOP Spacecraft

The science subsystem of the VSOP spacecraft, a block diagram of which is shown in Figure 2, processes the radio astronomy signal as follows. After a quarter wave plate combines the two orthogonal linear polarizations into LCP, the received radiation is sent down a coaxial cable in the case of the 1.6 GHz and 5 GHz bands, and a waveguide in the case of the 22 GHz to the Low Noise Amplifiers (LNAs). The LNAs have receiver noise temperatures of ≈ 35–40 K at 1.6 GHz/5 GHz and 150 K at 22 GHz, and gains of ≈ 35–40 dB. Unlike the case for ground-based VLBI antennas, there is relatively large (≈ 0.6 dB) attenuation between the feed and the LNAs, which are located on a plate that lies directly below the feed. Associated with this attenuation is a large contribution (≈ 40–50 K) to the overall VSOP spacecraft system temperature. The physical temperatures of the LNAs are expected to vary from −24°C to +13°C. The rest of the science subsystem is located on a solar panel side of the spacecraft main body, which is a good location for passive cooling of various components.

After the LNAs, the signals from each RF band are downconverted to IF, split into two paths, and sent to the IF switch. Two of the six input signals (two from each RF band), which in normal modes of operation will be from the same RF band, are then sent to the video converters. At this stage, there are two channels, referred to as channel A and channel B. Each video converter is an image rejection mixer (IRM) which converts the IF signal to baseband (0-32 MHz) as well as rejecting the lower side band image frequencies. The LO frequency for each of the two video converters can be chosen in integral MHz steps and can be independently set.

After the video converters, the A and B channel signals each pass through either 16-MHz or 32-MHz low pass filters, depending on which VSOP spacecraft observing mode has been selected. At this stage the A and B channel signal levels are sampled by square law detectors, the 12-bit digital outputs of which are sent to the main spacecraft computer, the data handling unit (DHU), to be subsequently sent down to the ground in the VLBI data headers. These power levels are used to determine the VSOP spacecraft system temperature and to monitor the sampler power levels. After this point, the A and B channel signals are one- or two-bit digitized, QPSK encoded onto the 14.2 GHz K_u-downlink carrier, further amplified, and sent to the K_u-band link antenna for transmission to a tracking station on the ground. The data rate of the downlink signal is 128 Mbps. The steerable K_u-band link antenna has a diameter of 45.5 cm and is located on a boom to improve tracking station communication.

The VSOP spacecraft does not have an on-board hydrogen maser frequency standard, but receives its reference signal from the ground as a 15.3 GHz tone derived from a hydrogen maser at a tracking station. This 15.3 GHz tone is received by the same K_u-link antenna that is used to transmit the 14.2 GHz downlink. The 15.3 GHz tone is sent to the K_u-band receiver, whose function is to search for, detect, and convert this tone into the fundamental 50 MHz reference signal for the spacecraft. The measured phase residuals in the two-way link signal will be used to correct the spacecraft clock and oscillators at

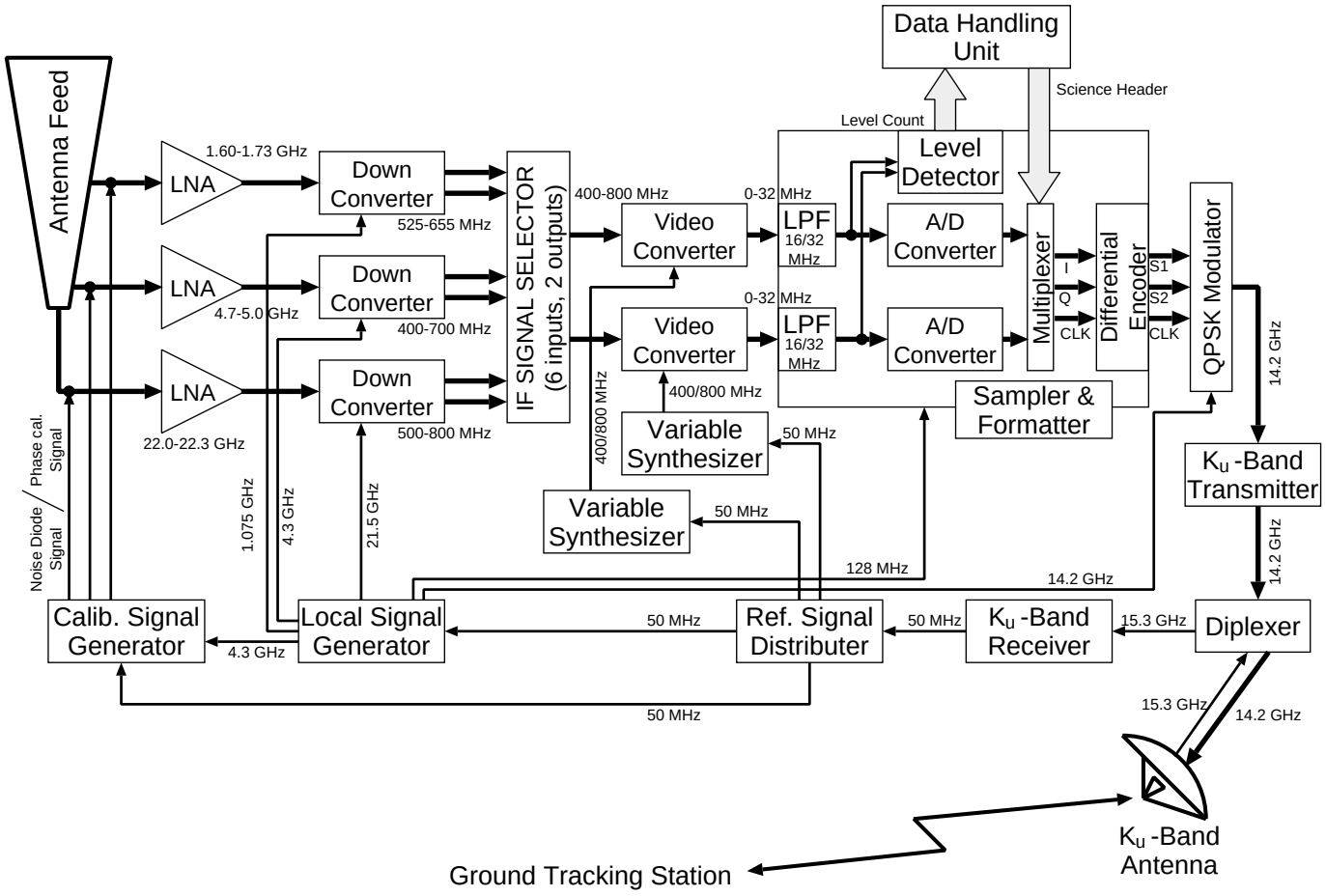

Figure 2: Diagram of the VSOP spacecraft science subsystem.

the correlator. In the absence of the 15.3 GHz tone the 50 MHz reference signal will be derived from an on-board crystal oscillator.

VSOP spacecraft system temperatures will be measured about every 10 minutes by switching on a noise diode for about 7 seconds and comparing the power level (at the point in the signal path just before the A/D converters) when the noise diode signal is injected in the LNA with the power level when the noise diode signal is not injected. By default, phase calibration tones every MHz throughout the observing band will be continuously switched on for continuum observations and switched off for spectral line observations. PIs can request on the VSOP proposal Cover Sheets that the tones be either switched on or off. Both the noise diode and phase calibration signals are injected through 25 dB couplers into the LNAs (see §13 for more details on VSOP spacecraft data calibration). The phase calibration tones will be extracted at the tracking stations.

The properties of the VSOP spacecraft antenna and science subsystem are summarized in Table 4. The three VSOP observing modes are shown in Table 5. It is important to note that only one of the three observing modes is VLBA/MkIV/S2 compatible (see §8 for a discussion of the different VLBI recording systems that will be supporting VSOP observations). It is only this observing mode that can be used when VSOP is co-observing with non-Japanese ground radio telescopes.

Table 4: Properties of the VSOP Spacecraft Science Subsystem

	Observing Band		
	1.6 GHz (20 cm)	5 GHz (6 cm)	22 GHz (1.35 cm)
Frequency Range (GHz)[1]	1.60–1.73[2]	4.7–5.0	22.0–22.3
Polarization	LCP only	LCP only	LCP only
Aperture Efficiency[3]	38%	54%	47%
Aperture Sensitivity (mK Jy^{-1})	69	98	85
System Temperature (K)	100	120	200
SEFD (Jy)[4]	14500	12200	23500

Notes:
1. The frequency range of each channel can be independently set such that the lower and upper frequencies of each channel are an integral number of MHz. The difference between the lower and upper frequencies of each channel must be equal to the channel bandwidth. Thus, for a 16 MHz channel, a frequency range of 1700-1716 MHz is okay, but both 1700.5-1716.5 MHz and 1700-1717 MHz are not.
2. Proposers who wish to observe the 1.72 GHz OH line should be aware that some ground radio telescopes, for example the VLBA, have difficulty supporting observations at 1.72 GHz due to the RFI environment.
3. The VSOP spacecraft main antenna has a hexagonal shape which has a total area of 50.1 m^2 and is thus equivalent to a circular antenna of diameter 8.0 m. The aperture efficiencies quoted here are based on a 50.1 m^2 aperture area .
4. The system equivalent flux density (SEFD), also known as the system temperature in Jy, is the ratio of the system temperature in K to the antenna sensitivity in K Jy^{-1}.

Table 5: VSOP Spacecraft Observing Modes

Mode properties			Recorder compatibility	
Number of channels	Bandwidth per channel	Sampling quantization	VLBA/MkIV/S2 compatible	VSOP terminal compatible
Two	16 MHz	2 bit	yes	yes
Two	32 MHz	1 bit	no	yes
One	32 MHz	2 bit	no	yes

4 VSOP Spacecraft Constraints

The VSOP spacecraft has a number of constraints which may make it impossible for the spacecraft to observe a given source under certain conditions. An understanding of the spacecraft constraints enables the proposer to understand what type of observations are feasible and what time scales are appropriate for monitoring observations.

4.1 Solar

The VSOP satellite cannot observe sources within 70° of the Sun. This constraint arises from the fact that the solar panels must be fully illuminated by the Sun to generate sufficient power for scientific observations. When a source is within 70° of the Sun the main antenna shadows the solar panels; they are therefore under-illuminated and cannot provide the required solar power.

4.2 Moon

The VSOP satellite cannot observe sources occulted by the moon.

4.3 Earth

Like ground radio telescopes, the VSOP spacecraft cannot observe sources occulted by the Earth. Unlike ground radio telescopes, which are fixed to the Earth, the varying altitude of the VSOP spacecraft means that the fraction of the sky occupied by the Earth varies. At the closest approach of the spacecraft to the Earth (perigee), the Earth occupies 25% of the celestial sphere, whereas at the furthest point from the Earth (apogee) the Earth only occupies 1.3% of the celestial sphere. Thus this constraint is much less severe for VSOP than it is for a ground radio telescope.

4.4 Eclipse

The VSOP satellite cannot observe when the Sun is occulted by the Earth. When this happens, the spacecraft has to use its batteries to power the spacecraft. Scientific observations are not possible during eclipse because they would cause too large a drain on the batteries. Figure 3 shows the VSOP spacecraft eclipse history using the nominal orbit shown in Table 6. As can be seen, there are periods of no eclipses, relatively long periods of short eclipses lasting $\approx$ 20 minutes and relatively short periods of long eclipses lasting $\approx$ 90 minutes. Eclipses produce gaps in (u,v) coverages that stay fixed from orbit to orbit on the timescale of a typical observation.

4.5 Tracking Network

The satellite is supported by a limited tracking network of 5 tracking stations (see §6 for more details). The high VLBI data rate (128 Mbps) requires that the VLBI data must be down-linked in real time. Therefore it is impossible for the satellite to observe if it is not above the minimum elevation limit of any tracking station. In addition, the satellite depends upon contact with a ground tracking station for its local oscillator phase reference.

4.6 Spacecraft Telemetry Horizon Mask

Even if all of the above constraints are met it may still be impossible to observe. The VSOP satellite has only one telemetry antenna to transmit the VLBI data to the tracking stations. The telemetry antenna is on a boom attached to the opposite side of the spacecraft main body from the main (8m) antenna. This telemetry antenna itself has a limited field of view, so it cannot communicate with a tracking station if, from the perspective of the telemetry antenna, the tracking station lies within $\approx$ 70°of the source direction. Thus in order to communicate with a tracking station the spacecraft must be above

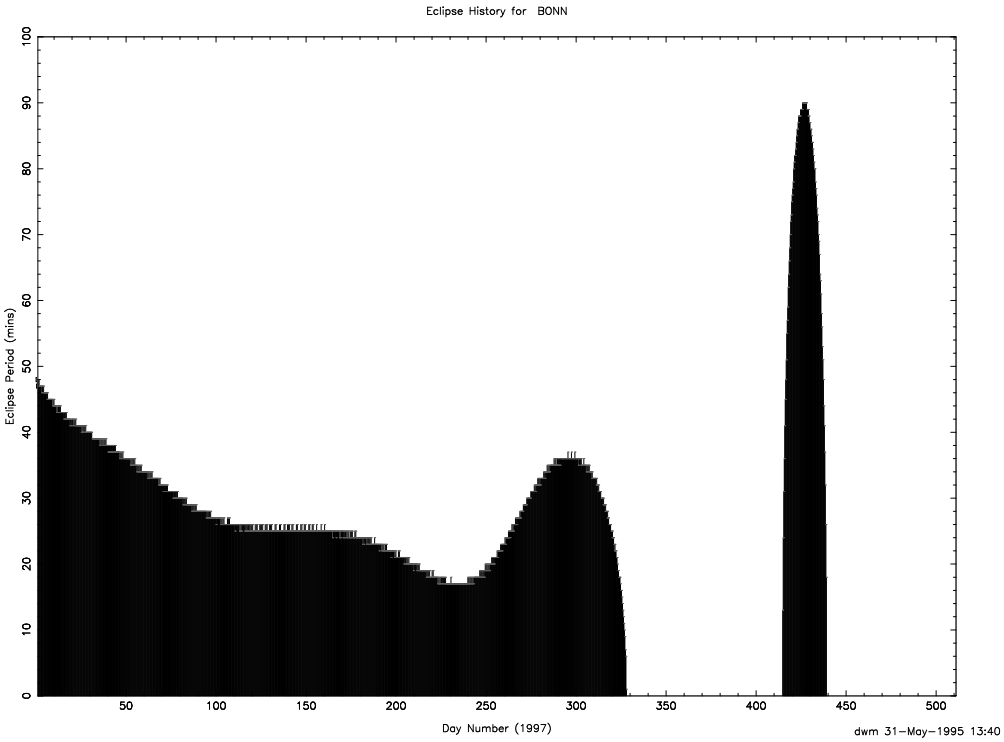

Figure 3: VSOP spacecraft eclipse history.

the minimum elevation limit of the tracking station and the tracking station must lie within the field of view of the telemetry antenna.

4.7 Slew Time and Settling

When changing sources, the VSOP satellite can slew at a rate of 2.25° min^{-1}. However, slewing is a two-stage process which means that the total angle the spacecraft slews through is larger than the angle between the two sources. The satellite first slews around the spacecraft-Sun axis followed by a slew about the solar-panel axis. Thus even under optimum conditions it will take 80 minutes to slew 180°. Furthermore, once the slew is completed it will take some time for the antenna to settle. Simulations show that the settling time is ≈ 5 minutes for 22 GHz observations and ≈ 3 minutes for observations at 1.6 and 5 GHz.

4.8 On-board Command Memory

Approximately once every four orbits (= 26.4 hours) the VSOP spacecraft will receive a new command sequence from the Kagoshima Space Center (see Table 7). This command sequence is composed of at most 256 commands, of which approximately 200 are devoted to scientific activities. One command is required for each of the following scientific activities: (1) to measure the system temperature (the system temperature is not measured continuously but at discrete intervals), (2) to change frequency band and/or LO settings, and (3) to change source. Thus there is a trade-off to be made between how frequently to change source, how frequently to change observing band and/or LO settings and how frequently to measure the system temperature. Furthermore it is only possible to observe a maximum of four sources in each command sequence. Although it takes only one command to change source, each source itself requires additional information that is used primarily by the star sensors in the attitude control subsystem. The one exception to the four sources rule is for sources separated by $< 3^\circ$. In this case it is possible to change sources using the attitude control subsystem, so that the new source is represented internally as

the old source with a pointing offset. Although this method may appear attractive for phase-referencing observations, it should be remembered that the settling time of the antenna needs to be taken into account and that the fractional baseline error is much higher for spacecraft-Earth than for the Earth-Earth baselines. Phase-referencing observations will not be possible at 5 or 22 GHz, and will be marginal at 1.6 GHz. Proposers who wish to use this method of changing sources should consult the VSOG by e-mail (vsog@vsop.isas.ac.jp) as to its technical feasibility.

5 VSOP Spacecraft Orbit

Space VLBI is simply ground VLBI with, in the case of the VSOP mission, an additional antenna in space. Since the science that can be produced by the VSOP mission is intimately tied to the VSOP spacecraft orbit, proposers need to be aware of the basic properties of orbits and how they change with time.

Table 6: Nominal VSOP Spacecraft Orbital Elements (Defined at 0 UT on 15 September 1996)

Keplerian Orbital Element	Value
a (semi-major axis)	17,878.14 km
ϵ (eccentricity)	0.587
i (inclination)	31.3°
Ω (right ascension of the ascending node)	77.4°
ω (argument of perigee)	105.5°
M (mean anomaly)	0.0°
Derived Parameters	
Orbital period	6.6 hours
Apogee height	22,000 km
Perigee height	1000 km

These orbital elements are for a launch date of 15 September 1996. The value of the mean anomaly is arbitrary as the exact sequence of perigee raising maneuvers is not yet known.

5.1 Definition of the Orbital Elements

To a good approximation, an orbit bound to the Earth is an ellipse with the Earth at one of the foci. It is convenient to refer to the orbit by the properties of this ellipse – the so-called six Keplerian orbital elements. Five of the six elements refer to the properties of the orbit ellipse and its orientation in space. The sixth element determines the location of the spacecraft on this ellipse. These elements, which are defined at a certain epoch, are:

a: Semi-major axis. The spacecraft orbital period, T, is related to the semi-major axis as follows $\mathrm{T} = 2.76\ (a/10^4\,\mathrm{km})^{3/2}$ hours.

ϵ: Eccentricity. The distance of the spacecraft from the center of the Earth at the closest approach to the Earth (perigee) is given by $a(1-\epsilon)$. The distance of spacecraft at furthest point from the center of the Earth in its orbit (apogee) is given by $a(1+\epsilon)$. To calculate the spacecraft height above the surface of the Earth at either perigee or apogee it is necessary to subtract the radius of the Earth from the previous expressions. The orbit semi-minor axis, b, is given by $a\sqrt{1-\epsilon^2}$.

i: Inclination. This is defined as $\cos^{-1}(L_z)$, where L_z is the component of the orbit unit angular momentum vector that lies along the Earth's rotation axis. For orbits that lie in the celestial

equator (equatorial orbits), $L_z = 1$, and hence $i = 0°$. For orbits perpendicular to the celestial equator (polar orbits), $L_z = 0$ and hence $i = 90°$.

Ω: Right ascension (or longitude) of the ascending node. Except for equatorial orbits, a spacecraft crosses the celestial equator twice every orbit: once when it is heading north and once when it is heading south. Ω is the right ascension of the spacecraft when it crosses the celestial equator heading north. This point is known as the ascending node. Like right ascension, Ω is usually measured in hours, but in some circumstances degrees is a more appropriate unit.

ω: Argument of perigee. This is defined as the angle in the orbital plane between the ascending node and perigee as measured from the center of the Earth. When ω is between 0° and 180° the perigee is in the northern hemisphere. Otherwise it is in the southern hemisphere.

M: Mean anomaly. Due to the conservation of angular momentum, the spacecraft moves at a non-uniform rate around the orbit ellipse. The angle between the spacecraft and perigee, as measured from the center of the Earth, is called the true anomaly. However it is convenient to work with another angle called the mean anomaly. If this is measured in degrees, the ratio M/360 is equal to the ratio of the time elapsed since the spacecraft last passed through perigee to the spacecraft orbital period. Thus, for a spacecraft at perigee, $M = 0°$, and for a spacecraft at apogee, $M = 180°$. For a spacecraft that moves in a circular orbit ($\epsilon = 0$) the mean anomaly and the true anomaly are the same.

The nominal VSOP spacecraft orbital elements are shown in Table 6.

5.2 Orbit Normal and (u,v) Coverages

The orientation of the orbital plane in space and the orientation of the orbit semi-major axis within the orbital plane control the type of (u,v) coverage that can be obtained for a given source. The orbit normal, which lies in the northern hemisphere, and the orbit anti-normal, which lies in the southern hemisphere, define directions along which the highest two-dimensional resolution observations will be obtained i.e., those observations for which the synthesized beam area is a minimum. The celestial coordinates (α, δ) of the orbit normal and the orbit anti-normal are (Ω−6h, 90°−i) and (Ω+6h, i−90°) respectively. For sources that lie in the orbital plane, that is 90° from the orbit normal, approximately linear (u,v) coverages are obtained.

Figure 4 shows an example of how the (u,v) coverage varies as a function of α and δ at a particular epoch. The case where the source is in the orbit plane can be clearly seen, since this is where linear (u,v) coverage is obtained. The large blank region in the set of (u,v) coverages is caused by the constraint that the VSOP spacecraft cannot observe within 70° of the Sun. This region of exclusion moves across the sky during the year. More examples of how the (u,v) coverages vary during AO phase 1 observations are shown in Appendix C. AO phase 1 observations cover a 17 month observing period beginning in January 1997 and ending in May 1998. Proposals for this observing period are covered by the first VSOP AO (please consult the VSOP AO for more details).

At apogee, for a source that lies along the orbit normal direction, the projected baseline lengths range from about 23,000 km to 33,000 km depending on the location of the ground radio telescopes with respect to the spacecraft. Since this lower limit exceeds the maximum baseline that can be obtained with ground-based VLBI arrays ($\approx$ 10,000 km) it inevitably follows that there will be large holes in the (u,v) plane for sources observed along or near the orbit normal (or anti-normal) direction. However, for sources that lie away from the orbit normal direction, the size of these (u,v) holes can be minimized by projection effects. Since (u,v) holes lead to image reconstruction errors there is an important trade-off to be made between image fidelity and resolution. Proposers who want the highest fidelity images will have to sacrifice some resolution and request observations in which the size of the (u,v) holes is minimized by projection effects. On the VSOP proposal Cover Sheets if proposers check the 'No holes (u,v) coverage' box then every attempt will be made to schedule their experiment under these conditions. Alternatively

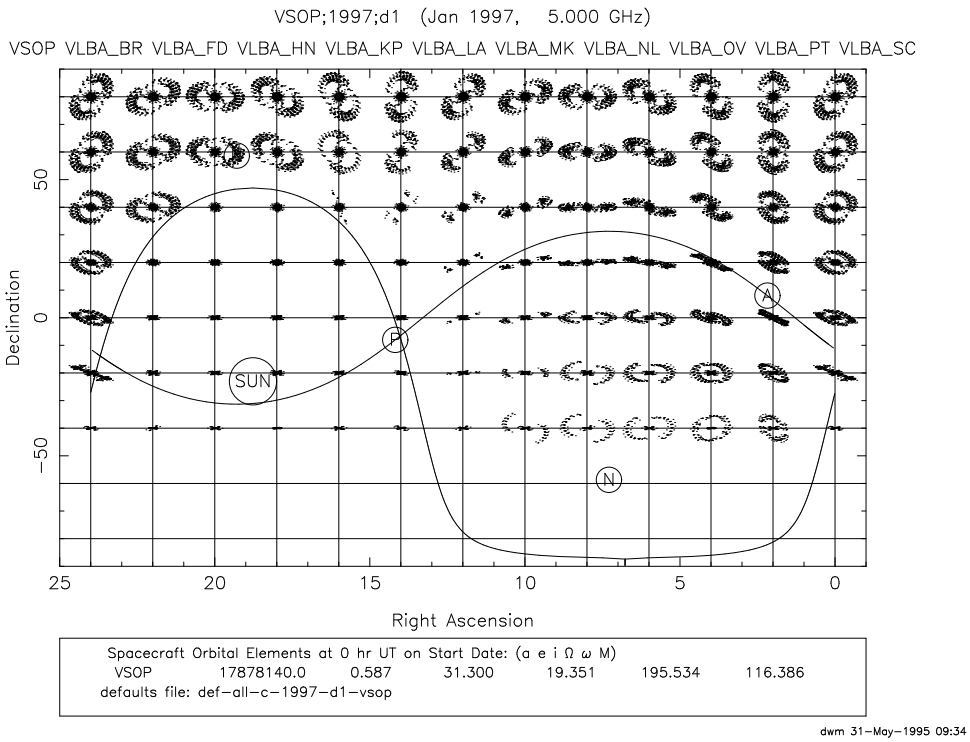

Figure 4: All-Sky (u,v) plot for the VSOP spacecraft with the VLBA on 1 Jan 1997.

proposers may want to obtain the maximum resolution. If they check the 'maximum resolution (u,v) coverage' box then every attempt will be made to satisfy this request during scheduling.

5.3 Precession of the Orbital Elements

Due to the oblateness of the Earth, the precession of the orbital elements ω and Ω has a significant impact on what (u,v) coverage can be obtained for a given source as a function of time. These precession rates are given by:

$$\dot{\Omega} = -752 \frac{\cos i}{(1-\epsilon^2)^2} \left(\frac{a}{10^4\ km}\right)^{-\frac{7}{2}} {}^\circ\ \mathrm{yr}^{-1} \tag{1}$$

$$\dot{\omega} = -\frac{1}{2}\left(\frac{5\cos^2 i - 1}{\cos i}\right)\dot{\Omega} \tag{2}$$

For the VSOP spacecraft in its nominal orbit (shown in Table 6) $\dot{\Omega} = -196^\circ\ \mathrm{yr}^{-1}$ and $\dot{\omega} = +304^\circ\ \mathrm{yr}^{-1}$. If the actual orbital elements differ from the nominal values, the actual precession rates will also differ from these nominal values (see §5.4 for more details).

5.3.1 Impact of Ω Precession

One major consequence of the Ω precession is that the direction of the orbit normal changes with time, and hence the directions in the sky for which the best (u,v) coverages are obtained also change with time. Figure 5 shows an example of how for a particular source, 1928+738, (u,v) coverages vary as a function of time. As can be seen, the (u,v) coverages change quite dramatically with time.

Plots like those shown in Figure 5 are particularly useful in planning monitoring observations (see §14 on proposal aid software).

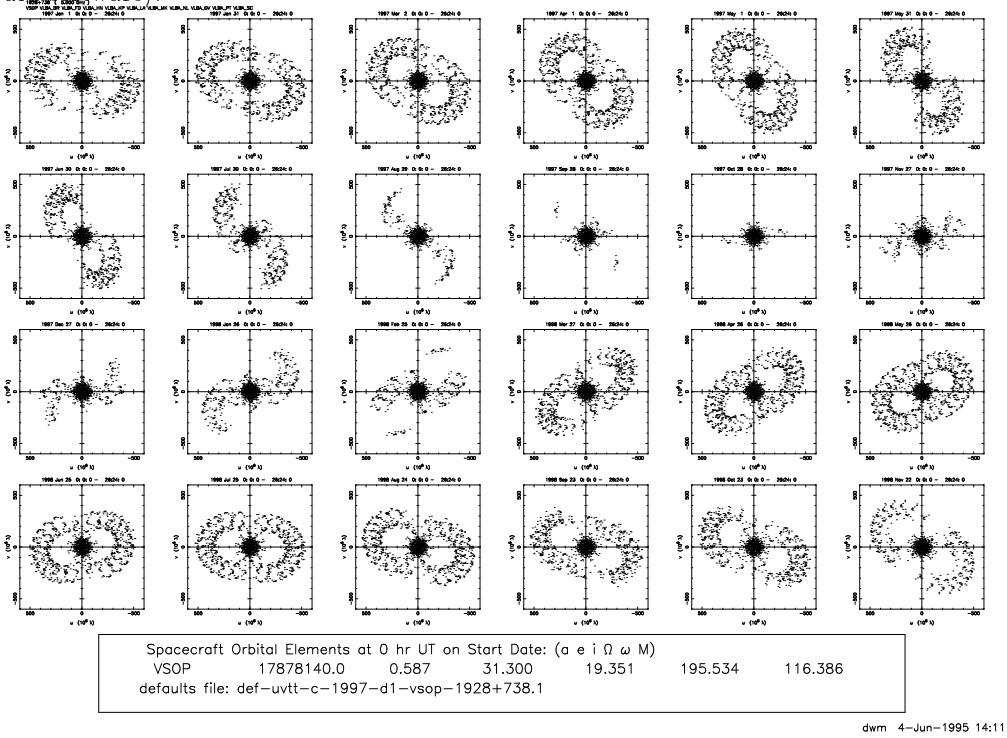

Figure 5: Example (u,v) plot as a function of time. (u,v) coverages for a 4 orbit observation of 1928+738 with the VSOP spacecraft and the VLBA, starting at the top left on 1 Jan 1997 and going from left to right with a (u,v) coverage produced once a month for a two year period.

5.3.2 Impact of ω Precession

One major consequence of the ω (and Ω) precession is that the position angle (PA) of the maximum projected baseline in the (u,v) coverage for a particular source changes with time. See Figure 5 for an example of this. Since the PA of the minor axis of the synthesized beam also lies along this PA it follows that the PA of the beam minor axis will also depend on the observation date. Proposers may want to observe a source with a preferred value of the PA of the beam minor axis. For example proposers might want more resolution along a VLBI jet than across the jet. In the VSOP proposal Cover Sheets proposers can specify the preferred PA of the beam *major* axis. Note that it is conventional to refer to the position angle of the beam *major* axis and not the PA of the beam minor axis. The PA of the beam major axis is at 90° to the PA of the beam minor axis and it is the PA along which there is the lowest resolution.

Another major consequence of the ω precession is that the amount of tracking available for the VSOP spacecraft, and hence the amount of space VLBI data that can be obtained during an observation, is a function of ω, and hence the epoch of the observation. The reason for this is that four of the five VLBI data acquisition tracking stations are located in the northern hemisphere (see Table 7). Hence more space VLBI data is obtained when the apogee of the orbit is in the northern hemisphere ($180° < \omega < 360°$) compared to when the apogee is in the south ($0° < \omega < 180°$). See §6 for more details on the tracking network.

Furthermore there is an interaction between the field of view of the VSOP spacecraft telemetry antenna and ω that limits the amount of tracking that is available for certain sources under certain conditions. For example, when apogee is in the northern hemisphere it is difficult to observe far southern sources at or near apogee, since under these conditions the telemetry antenna points away from the Earth and

cannot communicate with a tracking station (see §4.6).

5.4 Pre-Launch Uncertainty in the Orbital Elements

The VSOP satellite will be the first launch of the new ISAS M-V rocket. After launch, the satellite will be in an orbit with a nominal apogee height of 22,000 km and nominal perigee height of 215 km. Within the first week of operations the perigee height will be raised to 1000 km. However there is a range of potential launch dates from 5 September to 30 September which leads, with other launch constraints, to the actual value of Ω being up to $\pm$ 1 hr from the value given in Table 6. Furthermore the actual apogee height may vary by as much as $\pm$ 3000 km from its nominal value of 22000 km. This leads to a range in potential orbital periods from 5.8 hours to 7.5 hours, after the perigee height has been raised to 1000 km. The a priori apogee height uncertainty leads to a range of values of $\dot{\Omega}$ (in $^\circ\,\mathrm{yr}^{-1}$) from -167 to -235 and a range of values of $\dot{\omega}$ (in $^\circ\,\mathrm{yr}^{-1}$) from $+261$ to $+367$. Consequently, before launch, it is not possible to predict exactly when the optimum time will be to undertake a particular observation. Also, it is not known what the mean anomaly will be at the orbit reference epoch.

Proposers should use the nominal orbit listed in Table 6 when planning what observations are feasible. During the scheduling process, any differences between the nominal and actual satellite orbit will be taken into account when scheduling a particular observation.

6 VSOP Spacecraft Tracking Network

Table 7: VSOP Spacecraft Tracking Network

Commanding (S-band)				
Location	Latitude	Longitude	Recorder	Agency
Kagoshima, Japan	31°N	131°E	—	ISAS
VLBI Data Acquisition and Phase Transfer (K_u-band)				
Usuda, Japan	36°N	138°E	VLBA/VSOP	ISAS
Goldstone, California, USA	35°N	116°W	VLBA	NASA/JPL
Madrid, Spain	40°N	4°W	VLBA	NASA/JPL
Canberra, Australia	35°S	149°E	VLBA	NASA/JPL
Green Bank, West Virginia, USA	38°N	80°W	VLBA	NRAO

Unlike ground VLBI radio telescopes, whose hydrogen maser reference signal and VLBI data recorder are typically located close to the antenna, for the VSOP spacecraft these facilities are located at a tracking station many thousands of kilometers from the spacecraft. Two types of tracking stations support the VSOP spacecraft: (1) commanding stations (S-band), and (2) VLBI data acquisition and phase transfer stations (K_u-band). Table 7 lists the location of these tracking stations. The VSOP spacecraft will only be commanded from Kagoshima but there is an international network of 5 VLBI data acquisition and phase transfer stations to collect the VLBI data. It is important to note that 4 of these 5 tracking stations are in the northern hemisphere. Depending on the time-variable argument of perigee (ω) of the VSOP spacecraft orbit (see §5.3.2), the amount of time that the VSOP spacecraft is above the elevation limits of the VLBI data acquisition tracking stations varies from 55% of the time (for the worst case when $\omega = 90°$) to 85% of the time (for the best case when $\omega = 270°$). The VLBI data acquisition tracking stations will record the VLBI data on VLBA recorders, with the exception of Usuda that can record the data on either a VLBA or a VSOP terminal recorder. After the completion of an observation, the VLBI data will be shipped to the appropriate correlator. Various auxiliary data will be sent to the VSOG, which will create various auxiliary files and send them to the correlator. These files are needed both for correlation and subsequent data analysis. The VSOG will decide which tracking stations will track

the spacecraft and organize the sending of all the relevant VLBI and auxiliary data to the appropriate correlator. One impact of the tracking network is that it will be necessary to separately fringe fit each tracking station pass since a new and unpredictable delay offset is introduced at each tracking station hand-over.

7 Ground Radio Telescopes

The VSOP satellite will be a single element in a VLBI array. Without ground radio telescopes to co-observe with the satellite it is unable to perform its mission. Discussions among the directors of the world's ground observatories, under the auspices of the Global VLBI Working Group (GVWG), have resulted in the forward commitment of observing time, as shown in Table 8, to space VLBI. In order to facilitate greater scheduling efficiency, some of the EVN telescopes may be scheduled preferentially at certain observing bands. Hence the Lovell telescope at Jodrell bank has committed to observe 30% of all space VLBI observations at 1.6 GHz. Ground observatories which are not fully dedicated to VLBI, such as the EVN and ATNF telescopes (ATCA, Mopra, and Parkes) , prefer time to be allocated in blocks. It should also be noted that some observatories have especially high program pressure at certain times of year (e.g., Effelsberg during night time in May through July when the Galactic Center observations may take preference). For each telescope, Table 8 also shows the system equivalent flux densities (SEFDs) for the three VSOP observing bands, the telescope diameter, the VLBI recording system (or systems), and other information needed by proposers when they fill in the VSOP proposal Cover Sheets. This information includes a two letter code used to refer to an individual telescope and the classification of the telescope as medium or large (as defined in a footnote to the table) as a function of observing band. For comparison purposes the SEFDs for the VSOP spacecraft are shown at the bottom of this table. The system temperatures are the current best estimates for late 1996 and are subject to change. The percentage time commitment is the percentage of the number of hours in the year that the particular telescope will commit to space VLBI observations. During AO phase 1 observations it is likely that the VSOP mission will be the only space VLBI mission. During AO phase 2 observations the VSOP mission may have to share observing time with the Russian RadioAstron mission, if RadioAstron is operational at that time. Time commitments given as UN are still under negotiation. Time commitments given as a percentage followed by an asterisk (e.g. Arecibo) have been agreed to but are dependent on funding to either operate the observatory or to purchase relevant equipment (e.g. hydrogen maser or VSOP compatible VLBI recorder) to support space VLBI observations. If there is a question mark after a recorder it means there are plans but no definite budget to purchase that type of recorder.

8 VLBI Recording Systems

The tracking stations and ground radio telescopes used to support the VSOP mission will use four different recording systems to record the VLBI data. These recording systems are: VSOP, VLBA, MkIV and S2. Only one of the three VSOP observing modes, the mode with two 16 MHz two-bit sampled channels (see §3), can be supported by the VLBA, MkIV and S2 systems. The Usuda tracking station is equipped with both VSOP and VLBA recorders; the other VLBI data acquisition tracking stations are equipped with VLBA recorders only. These recording systems use different physical media and it is a non-trivial exercise to cross-correlate data recorded on different recording systems with one another (see §12.1 for more details).

9 Observational Capabilities of the VSOP Mission

In this section the proposer is provided with the necessary information to calculate the resolution, the baseline sensitivity, the image sensitivity, and the field of view that one can obtain with VLBI observations

Table 8: Participating Ground Radio Telescopes and VLBI Networks

GRT/Network	Code[1]	Location	Size[2]	Diam. (m)	SEFD (Jy)[3] 1.6 GHz	5 GHz	22 GHz	Recorder	Time[4]
Arecibo	AR	Puerto Rico	LL-	305	2.5	3.5	—	S2	4%*
EVN:	EVN	Europe/Asia						MkIV, VLBA	
Effelsberg	EF	Germany	LLL	100	19	44	127	VLBA/MkIV	11%
Jodrell (Lovell)	JO	UK	L--	76	44	—	—	MkIV	∼5%
Jodrell (Mk II)	JO	UK	-MM	26	—	320	910	MkIV	10%
Medicina	MC	Italy	MMM	32	1176	284	1084	MkIV	20%
Metsahovi	MH	Finland	--M	14	—	—	2600	VLBA	25%
Noto	NO	Italy	MMM	32	784	187	1225	VLBA	15%
Onsala	ON	Sweden	--M	20	—	—	1597	MkIV	5%
Onsala	ON	Sweden	MM-	25	394	1000	—	MkIV	20%
Shanghai	SG	China	MMM	25	1176	467	2419	VLBA,S2	25%
Simeiz	SM	Ukraine	MMM	22	1848	3036	1000	MkIV?	15%*
Torun	TR	Poland	MM-	32	240	240	—	MkIV	15%
Urumqi	UR	China	MMM	25	990	934	2419	MkIV?,S2?	25%*
WSRT	WB	Netherlands	ML-	14x25	120	108	—	MkIV	15%
Goldstone[6]	GO	USA	L-L	70	49	—	65	MkIV	11%
Green Bank	NR	USA	LLM	43	75	130	400	VLBA	<8%
Hartebeesthoek	HT	South Africa	MM-	26	420	970	—	MkIV, S2?	UN
Hobart	HO	Australia	MMM	26	550	550	1500	S2	10%*
Kashima	KA	Japan	MMM	34	231	365	1356	VSOP, MkIV	UN
Madrid[6]	RO	Spain	L-L	70	49	—	65	MkIV	11%
Mopra	MR	Australia	MMM	22	350	450	1000[5]	S2	25%
Narrabri (ATCA)	CG	Australia	LLL	6x22	60	80	170[5]	S2	∼5%
Nobeyama	NB	Japan	--L	45	—	—	217	VSOP/VLBA	∼10%
Parkes	PA	Australia	LLM	64	50	90	600	S2	∼5%
Tidbinbilla[6]	TI	Australia	L-L	70	49	—	65	MkIV, S2	11%
Usuda	UD	Japan	LL-	64	69	69	?	VSOP, VLBA	UN
VLA-27	VL	USA	LLL	27x25	13	14	78	VLBA	<3%
VLBA[7]	VLBA	USA	MMM	10x25	298	296	930	VLBA	30%
Spacecraft									
VSOP	—	in orbit	---	8	14500	12200	23500	—	—

1. The two letter codes used to represent individual telescopes with the exception of the codes VLBA and EVN that indicate the entire VLBA or EVN arrays that operate at a given frequency. These code letters must be used when specifying ground arrays of individual telescopes or the VLBA and EVN arrays in the VSOP proposal Cover Sheets.
2. The size of a particular telescope at each of the VSOP observing bands. M = medium antenna and L = large antenna. At 1.6 GHz, 5 GHz and 22 GHz the SEFD[3] break points between a medium and large antenna are 100 Jy, 150 Jy and 300 Jy respectively. In the proposal Cover Sheets proposers may specify instead of individual telescopes how many medium and large antennas they need in their ground array.
3. The system equivalent flux density (SEFD), also known as the system temperature in Jy, is the ratio of the system temperature in K to the antenna sensitivity in K Jy^{-1}.
4. This column is the percentage of time that each telescope or array has committed to supporting the VSOP mission during AO phase 1 observations. This number may change once the proposals for AO phase 1 observations have been submitted and the quality of science with the VSOP mission can be directly compared to ground-based observing programs. Time commitments given as a percentage followed by an asterisk have been agreed to but are dependent on funding to either operate the observatory or to purchase relevant VLBI equipment.
5. 22 GHz system unlikely to be implemented until 1998.
6. It is expected that one of the three DSN sites will be equipped with MkIV by September 1996, with the other two ready 6 to 9 months later.
7. Unlike the linked interferometers listed in this table (Narrabri, VLA-27, and WSRT) the SEFD numbers quoted here are for an individual VLBA antenna, not for the phased array. The reason that there are not 10 entries in this table, one for each VLBA antenna, is if proposers want to use VLBA antennas, they must request use of the entire 10 element array by using the code VLBA in the VSOP proposal Cover Sheets (see §11.2).

using the VSOP satellite and co-observing ground radio telescopes. There is also a discussion of the polarization and spectral line capabilities of the VSOP mission.

9.1 Resolution

The resolution for an observation depends on the orientation of the source with respect to the orbit normal. For a source that lies along the direction of the orbit normal (or anti-normal), the full width half maximum (FWHM) beam size along the direction of the beam minor axis, $\theta_{\rm minor}$, is related to the observing frequency, ν, as follows:

$$\theta_{\rm minor} \approx 1.2 \left(\frac{\nu}{GHz}\right)^{-1} \text{mas} \tag{3}$$

Similarly the FWHM beam size along the direction of the beam major axis, $\theta_{\rm major}$, is related to the observing frequency, ν, as follows:

$$\theta_{\rm major} \approx 2.3 \left(\frac{\nu}{GHz}\right)^{-1} \text{mas} \tag{4}$$

For sources that do not lie along the orbit normals, the FWHM major and minor beam sizes will be greater than or equal to the values quoted above. Furthermore the above beam sizes are those for an observation with the VSOP spacecraft and the VLBA using uniform weighting with each visibility weighted by the RMS noise level to the power $-\frac{1}{4}$. The beam size is a function primarily of the orientation of the source with respect to the orbit normal and the weighting scheme used. It depends only secondarily on the ground array used. It should also be noted that the FWHM minor axis beam size quoted above is 65% of the size of the fringe spacing for the longest baseline. This is quite consistent with the weighting scheme used.

Example: For a VSOP observation at 5 GHz, in the direction of the orbit normal, $\theta_{\rm minor} = 0.24$ mas and $\theta_{\rm major} = 0.46$ mas.

9.2 Baseline Sensitivity

The RMS thermal noise (σ_{ij}) in the visibility amplitude of a single polarization on a baseline between the i-th and j-th antennas in a VLBI array is given by:

$$\sigma_{ij} = (\eta_s^{-1}) \sqrt{\frac{T_i(Jy) T_j(Jy)}{2B\tau}} \tag{5}$$

where:

η_s = The VLBI system efficiency factor (always < 1). This factor accounts for losses in the VLBI system (e.g. quantization in the data recording and correlator approximations). For 1-bit (2 level) sampling the VLBI efficiency factor is 0.64 while for 2-bit (4 level) sampling this factor is 0.88 (assuming that correlator losses are small).

$T_i(Jy)$ = The SEFD (system temperature in Jy) for the i-th antenna. See Table 8 for the value of this parameter.

$T_j(Jy)$ = The SEFD (system temperature in Jy) for the j-th antenna. See Table 8 for the value of this parameter.

B = The bandwidth in Hz. For VSOP continuum observations the value of this parameter is either 32 or 64 MHz (see Table 5 for more details).

τ = The integration period in seconds. For fringe-fitting calculations, τ is the fringe-fitting interval. This should be about equal to the coherence time. See Table 9 for estimated values of the coherence time. For visibility data, τ is the integration period of each visibility point. This integration period can be, and often is, smaller than the coherence time.

Example: At 5 GHz, σ_{ij} is 15 mJy for the VSOP spacecraft to a single 25m VLBA antenna (assuming $T_{\rm VSOP}$ = 12200 Jy, $T_{\rm VLBA}$ = 296 Jy, B = 32 MHz, τ = 350 s and η_s = 0.88).

Example: At 5 GHz, σ_{ij} is 6 mJy for the VSOP spacecraft to the 100m Effelsberg antenna (assuming $T_{\rm VSOP}$ = 12200 Jy, $T_{\rm Effelsberg}$ = 44 Jy, B = 32 MHz, τ = 350 s and η_s = 0.88).

Table 9: Expected (90%) Coherence Times (τ).

Observing Band	1.6 GHz	5 GHz	22 GHz
τ (seconds)	650	350	150

9.3 Fringe Fitting Signal to Noise Ratio

When fringe fitting VLBI data, the signal to noise ratio (SNR) on the baseline between the i-th and j-th telescopes in a VLBI array, SNR$_{ij}$, is given by:

$$\mathrm{SNR}_{ij}(\tau) = \frac{C(\tau) S_c}{\sigma_{ij}(\tau)} \qquad (6)$$

where $C(\tau)$ is the coherence function, S_c is the correlated flux density of the source and $\sigma_{ij}(\tau)$ is the RMS noise level, given by Equation 5. Over the fringe-fitting interval, τ, the amplitude of the correlated signal is degraded due to atmospheric irregularities and noise in the frequency standards. C(τ) measures this degradation. To obtain the highest signal to noise when fringe fitting, the fringe fitting interval needs to be chosen such that the SNR, given by Equation 6, is a maximum. A reasonable choice of τ is that for which C(τ) = 0.9. Table 9 shows the values of this interval as predicted by Linfield and Kahn (1994), for the three different VSOP observing bands. Note that Equation 6 requires that the correlated flux density be used and not the total source flux density. Section 9.5 gives a method of how the correlated flux density can be predicted for Earth-space baselines.

Example: At 5 GHz, the SNR is 34 between the VSOP spacecraft and a single VLBA antenna for a 1 Jy circular Gaussian source with a brightness temperature of 1.22×10^{12} K observed on a projected baseline of 25,000 km (assuming $T_{\rm VSOP}$ =12200 Jy, $T_{\rm VLBA}$ = 296 Jy, B = 32 MHz, τ = 350 s, $C(\tau)$ = 0.9, and η_s = 0.88). See Equation 11 for how to calculate the correlated flux density.

Example: At 5 GHz, the SNR is 90 between the VSOP spacecraft and the 100m Effelsberg antenna for a 1 Jy circular Gaussian source with a brightness temperature of 1.22×10^{12} K observed on a projected baseline of 25,000 km (assuming $T_{\rm VSOP}$ =12200 Jy, $T_{\rm Effelsberg}$ = 44 Jy, B = 32 MHz, τ = 350 s, $C(\tau)$ = 0.9, and η_s = 0.88). See Equation 11 for how to calculate the correlated flux density.

9.4 Fringe Detection Limit

One important step in the processing of VLBI data after correlation is that the data must be fringe fit. In fringe fitting data, for ground-based VLBI, a search is made in delay and delay-rate space to find the fringe. For Space VLBI it may also be necessary to search in the delay-acceleration dimension as well. If the search space is large then a high minimum SNR is required to guard against the probability of false fringe detection. For space VLBI the size of the search space is critically dependent on the size of the position, velocity and acceleration errors in the VSOP spacecraft orbit. Ulvestad (private communication) has shown that, for a VLBI experiment with the VSOP spacecraft, the minimum SNR required to detect fringes is:

$$\boxed{\mathrm{SNR}_{\min} = 7} \tag{7}$$

Proposers need to convince themselves and the Scientific Review Committee that there is reasonable chance that SNR_{ij} will exceed $\mathrm{SNR}_{\min}$ on baselines to the VSOP spacecraft having projected lengths of order 25,000 km.

9.5 Estimated Correlated Flux Density

The SNR formula (Equation 6) requires that the correlated flux density, S_c, be used. Except for a point source, the correlated flux density is always less than the total flux density of the source. Thus, in order to predict if fringes will be detected on baselines to the VSOP spacecraft, we need a method of predicting the correlated flux density on these baselines. In the two methods described below, we treat the source as a single Gaussian component. In reality it is known that VLBI sources in general have complex morphology. Therefore the methods described below should be applied to the most compact VLBI component in a VLBI source, which for most extragalactic sources is the radio core.

9.5.1 Using the Source Size

If we assume that the source has a circular Gaussian brightness distribution, then the correlated flux density, S_c, measured on a projected baseline of length D is related to the total source flux density, S_0, and the full width half maximum size of the source, θ_{FWHM}, as follows:

$$\boxed{S_c = S_0 e^{-0.093(\frac{D}{10^4\ km})^2(\frac{\theta_{FWHM}}{1\ mas})^2(\frac{\nu}{1\ GHz})^2}} \tag{8}$$

Example: At 5 GHz, the correlated flux density is 0.56 Jy for a 1 Jy circular Gaussian source with $\theta_{FWHM} = 0.2$ mas observed on a projected baseline length of 25,000 km.

9.5.2 Using the Source Brightness Temperature

A useful way to characterize the monochromatic surface brightness of a radio source is to determine the physical temperature that a black body radiator would need to possess to produce the same observed surface brightness. This temperature is known as the brightness temperature of the radio source. For a circular Gaussian source the maximum brightness temperature, T_b, is related to the component flux density, S_0, the component full width half maximum size, θ_{FWHM}, and the observing frequency, ν, as follows:

$$\boxed{T_b = 1.224 \times 10^{12}(\frac{S_0}{1\ Jy})(\frac{\theta_{FWHM}}{1\ mas})^{-2}(\frac{\nu}{1\ GHz})^{-2}\ \mathrm{K}} \tag{9}$$

Example: At 5 GHz, the brightness temperature is 1.22×10^{12} K for a 1 Jy circular Gaussian source with $\theta_{FWHM} = 0.2$ mas.

Alternatively if the source brightness temperature is known and the source is again assumed to be a circular Gaussian, Equation 9 may be inverted to solve for the component full width half maximum size, θ_{FWHM}, in terms of the maximum brightness temperature, T_b, the component flux density, S_0, and the observing frequency, ν, as follows:

$$\theta_{FWHM} = 1.106 \, (\tfrac{S_0}{1\,Jy})^{\frac{1}{2}} (\tfrac{T_b}{10^{12}\,K})^{-\frac{1}{2}} (\tfrac{\nu}{1\,GHz})^{-1} \text{ mas} \tag{10}$$

Assuming a circular Gaussian source brightness distribution, the correlated flux density, S_c, is related to the brightness temperature, T_b, projected baseline length, D, and the observing frequency, ν, as follows:

$$S_c = S_0 \, e^{-0.114 (\frac{S_0}{1\,Jy})(\frac{D}{10^4\,km})^2 (\frac{T_b}{10^{12}\,\mathrm{K}})^{-1}} \tag{11}$$

Example: At 5 GHz, the correlated flux density is 0.56 Jy for a 1 Jy circular Gaussian source with a brightness temperature 1.22×10^{12} K observed on a projected baseline of 25,000 km.

The equations presented above (8 and 11) should not be taken as the definitive answer of what the correlated flux density will be on baseline lengths exceeding an Earth diameter. These equations are if anything a conservative approximation. Results from the TDRSS space VLBI experiments (§10.1) and ground-based VLBI have shown that a common property of radio sources is that they often have more correlated flux density on long baselines than is obtained by extrapolating simple Gaussian models derived from short baseline data.

9.6 Field of View

The field of view of a VLBI observation is limited by three effects which are examined in the following three subsections:

9.6.1 Non-Coplanar Phase Residuals

For a non-coplanar VLBI array, such as the VSOP spacecraft co-observing with a ground array, there is a contribution to the phase that depends on the square of the angular distance of the source away from the phase center. This extra phase is not corrected for in the standard algorithms used to process VLBI data. In order that this term does not become significant it is required to be less than 0.1 radians. This places a limit on the field of view, θ_{nc}, that is a function of both the observing frequency, ν, and the baseline length, D, as follows:

$$\theta_{nc} = 13000 \, (\tfrac{\nu}{1\,GHz})^{-\frac{1}{2}} (\tfrac{D}{10^4\,km})^{-\frac{1}{2}} \text{ mas} \tag{12}$$

Example: At 5 GHz for a baseline of 25,000 km, the field of view is limited to be less than 3.6 arcseconds due to this effect. Therefore this effect is insignificant.

9.6.2 Bandwidth Smearing

Due to the finite observing bandwidth, the visibility amplitude of a point source not located at the phase center is degraded. In order that this degradation is limited to only $P\%$, the limit on the field of view, θ_B, that is a function of both the observing bandwidth, B, and the baseline length, D, is as follows:

$$\theta_B = 60\, P^{\frac{1}{2}} \left(\frac{B}{16\ MHz}\right)^{-1} \left(\frac{D}{10^4\ km}\right)^{-1} \text{mas} \tag{13}$$

Example: If the visibility amplitude is to be degraded by less than 5%, the field of view is limited to less than 27 mas by this effect for an observation with a bandwidth of 32 MHz on a baseline of 25,000 km.

9.6.3 Time Average Smearing

Due to the finite integration time of each visibility point, the visibility amplitude of a point source not located at the phase center is degraded. The general analysis for ground VLBI is difficult and is often restricted for simplicity to a source located at the north (or south) pole. For space VLBI there is an analogy to the ground north pole case, and that is to consider a source located along the orbit normal. Due to the different spacecraft velocities at apogee and perigee, the fields of view are different at these two locations and we will consider both cases. The spacecraft velocity at apogee, V_a, and at perigee, V_p, depend on the spacecraft orbital period, T, orbit eccentricity, ϵ, and orbit semi-major axis, a, as follows:

$$\mathrm{V}_a = \frac{2\pi a}{T}\sqrt{\frac{(1-\epsilon)}{(1+\epsilon)}} \text{ and } \mathrm{V}_p = \frac{2\pi a}{T}\sqrt{\frac{(1+\epsilon)}{(1-\epsilon)}} \tag{14}$$

Example: V_a and V_p are 2.4 $\mathrm{km\,s^{-1}}$ and 9.3 $\mathrm{km\,s^{-1}}$ respectively for the nominal VSOP spacecraft orbit listed in Table 6.

In order that the visibility amplitude degradation due to time average smearing is limited to only P%, the limit on the field of view at either apogee or perigee, θ_τ, is a function of the observing frequency, ν, the visibility integration period, τ_v, and the spacecraft velocity, V, is as follows:

$$\theta_\tau = 96\, P^{\frac{1}{2}} \left(\frac{\nu}{1\ GHz}\right)^{-1} \left(\frac{\mathrm{V}}{1\ kms^{-1}}\right)^{-1} \left(\frac{\tau_v}{100\ sec}\right)^{-1} mas \tag{15}$$

Example: If the degradation to the visibility amplitude is to be less than 5%, the field of view is limited to be less than 5.1 mas at apogee for a visibility integration period of 350 seconds at 5 GHz. The corresponding limit on the field of view at perigee is 1.3 mas.

Both at apogee and perigee time average smearing is the major limitation on the field of view. In order to obtain the same field of view at perigee as at apogee it is necessary that the perigee integration time be smaller than the apogee integration by a factor that is equal to the ratio of the spacecraft apogee and perigee velocities. For the example used above this ratio is 3.9 and in order to have the same field of view at perigee as at apogee the perigee integration period must be reduced from 350 seconds to 90 seconds. It should also be pointed out that the time average example quoted here is for the worst, although not un-typical, case since it is along the orbit normal direction that the highest resolution observations will be obtained. Reducing the integration period of the visibility data compared to the time interval used for fringe fitting is quite acceptable since the SNR required to detect fringes is a factor of ≈ 2 higher than that needed to successfully image the data. Furthermore since there will in general be a higher correlated

flux density at perigee compared to apogee it is not unreasonable to have a shorter visibility integration period at perigee compared to apogee.

Another way of analyzing the field of view is to compare it to the size of the synthesized beam. For this calculation we will make the approximations that the synthesized beam is given by 0.65 λ/D (where λ = the observing wavelength and D = the maximum projected baseline length) and that time average smearing is the dominant limitation on the field of view. In this case the field of view measured in beams, $N_{\rm beams}$, is given by:

$$N_{\rm beams} = 25\ P^{\frac{1}{2}}(\frac{D}{10^4\ km})(\frac{\rm V}{1\ kms^{-1}})^{-1}(\frac{\tau_v}{100\ sec})^{-1}\ mas \tag{16}$$

Example: If the visibility amplitude is to be degraded by less than 5% and the maximum projected baseline length is 25,000 km, the field of view will be limited to 16 synthesized beams in size for visibility integration periods of 350 seconds at apogee and 90 seconds at perigee.

9.7 Imaging Sensitivity

Proposers wishing to make images need to work out if the expected RMS noise level on their images is low enough for them to meet the scientific goals of their experiment.

The RMS noise per beam on an image (for natural weighting), ΔI, is given by:

$$\Delta I = \frac{\sqrt{\sum w_{ij}^2 \sigma_{ij}^2}}{\sum w_{ij}} \tag{17}$$

where the summation is over all the visibilities in the experiment and w_{ij} is the weight attached to each visibility point and σ_{ij} is the RMS noise level on the visibility amplitude given by Equation 5. For a VLBI array of equal elements, it is easy to show that:

$$\Delta I = \frac{\sigma_{ij}}{\sqrt{N}} \tag{18}$$

where N is the number of visibility points and σ_{ij} is again the RMS noise level on the visibility amplitude. For an observation of a circumpolar source with an array of equal elements the above equation can be re-expressed in terms of the SEFD of an individual array element, T_i, the length of the observation, τ_{obs}, the bandwidth, B, the number of telescopes in the array, n_t, and the VLBI system efficiency factor, η_s, as follows:

$$\Delta I = \eta_s^{-1} \frac{T_i}{\sqrt{n_t(n_t-1)B\tau_{obs}}} \tag{19}$$

Example: At 5 GHz, for a VLBA-only (n_t=10) experiment on a circumpolar source that lasts 18 hours, ΔI= 25 μJy per beam (assuming $T_{\rm VLBA}$ = 296 Jy, B = 32 MHz, τ = 350 s and η_s = 0.88).

The extension of Equation 19 to an array of non-equal elements, like the EVN or the addition of the VSOP spacecraft to the VLBA say, is as follows. For such an array we can define a single SEFD number, $< T_i >$, such that the above equation is true for the array, if we substitute $< T_i >$ for T_i. It can be shown that $< T_i >$ is given by:

$$< T_i >= \sqrt{n_t(n_t-1)}\frac{\sqrt{\sum_i \sum_{j\neq i} (T_i T_j)^{1-m}}}{\sum_i \sum_{j\neq i} (T_i T_j)^{-\frac{m}{2}}} \tag{20}$$

In deriving the above expression the weight attached to each visibility point is chosen to be inversely proportional to the RMS noise raised to some power m ($w_{ij} = \sigma_{ij}^{-m}$). For optimum weak source detection $m = 2$. However many VLBI astronomers choose $m = \frac{1}{4}$ for VLBI arrays that contain antennas with a wide range of SEFD values. There is a trade-off to be made for space VLBI as to what is the best value to choose for m. With a lower value of m higher resolution images will be obtained but the beam side-lobe level and the image noise level will be higher.

Example: For the EVN antennas listed in Table 8 (excluding Simeiz and Urumqi as these antennas may not have recorders compatible for observations with the VSOP mission), and using Equation 20, it can be shown that for $m = 1/4$, $< T_i > = 380$ Jy (n_t=10), 305 Jy (n_t=10) and 1170 Jy (n_t=8) at 1.6 GHz, 5 GHz, and 22 GHz respectively. As the number of elements in the EVN array and the $< T_i >$ values are similar to the values for the VLBA the noise level obtained with a ground observation only with the EVN is similar to what is obtained with the VLBA. The error made by using the simple average for the EVN, $1/n_t \sum_i T_i$ as an approximation to $< T_i >$, is to overestimate this value by $\approx 25\%$ for $m = 1/4$.

There is a useful extension to Equation 20 and that is to consider the addition of the VSOP spacecraft to a ground array. In that case, the RMS noise level on the image, ΔI_{space}, is related to the RMS noise level obtained with the ground array alone, ΔI_{ground}, as follows:

$$\Delta I_{space} = \Delta I_{ground}\frac{\sqrt{1+\frac{2}{n_g-1}\left(\frac{T_v}{<T_g>}\right)^{1-m}}}{\left(1+\frac{2}{n_g-1}\left(\frac{T_v}{<T_g>}\right)^{-\frac{m}{2}}\right)} \tag{21}$$

where n_g is the number of the antennas in the ground array and $\frac{T_v}{<T_g>}$ is the ratio of the VSOP spacecraft SEFD to the ground array SEFD, calculated using Equation 20. In the above expression the weight attached to each visibility point is chosen to be inversely proportional to the RMS noise raised to some power m ($w_{ij} = \sigma_{ij}^{-m}$).

Example: At 5 GHz for a VLBA experiment with the VSOP spacecraft of a circumpolar source that lasts 18 hours, assuming that the source is always visible for VSOP, $\Delta I_{space} = 25$ μJy per beam for $m = 2$ and 46 μJy per beam for $m = \frac{1}{4}$ (assuming $T_{\rm VLBA} = 296$ Jy, $T_{\rm VSOP} = 12200$ Jy, $B = 32$ MHz, $\tau = 350$ s and $\eta_s = 0.88$).

9.8 Dynamic Range

The dynamic range of an image is defined as $P_+/\Delta I_m$, where P_+ is the peak flux density in the image in units of Jy/beam and ΔI_m is the measured RMS noise level on the image also in units of Jy/beam. It should be noted that the definition of dynamic range uses the measured image RMS noise level (ΔI_m) and not the theoretical number (ΔI) calculated using Equation 17. In VLBI images ΔI_m can be significantly higher than ΔI. For example, if the measured noise on the image was equal to the predicted thermal noise then the dynamic range in the previous example for a 1 Jy point source would be $\approx$ 20,000:1. Until recently, such a high dynamic range had never been achieved in a VLBI image. One of the main reasons for this is that the RMS noise level on a visibility point can exceed the thermal noise level predicted by Equation 5. One of the main causes for this is amplitude calibration errors. In VLBI amplitudes are typically calibrated to a few percent. Consider the case of an observation of a 1 Jy point source with each

visibility point having 5% amplitude errors (1 σ) distributed as a Gaussian about the true 1 Jy value. In this case σ_{ij} would be 50 mJy. For an observation with the VSOP spacecraft and a 10 element ground array for 18 hours the number of visibility points is $\approx 10^4$, assuming a visibility integration period of 350 seconds. Hence according to Equation 18 the RMS noise level on the map is expected to be ≈ 0.5 mJy and the dynamic range is this case would be $\approx$ 2000:1. Calibrating the VSOP spacecraft antenna will be very different from what is normally encountered in ground-based VLBI (see §13 for details) and it will be during the in-orbit checkout phase of the mission, before AO phase 1 observations begin, that the properties of the antenna will be determined. Proposers should therefore proceed with caution when estimating the dynamic range that will be achieved. The actual dynamic range achievable may be a factor of 10 worse than predicted by using thermal noise calculations such as Equation 17.

9.9 Typical VSOP Observations

For ground-based VLBI, (u,v) coverages repeat every 24 hours. Since the expected ratio of the VSOP spacecraft orbital period (6.6 hours) to the Earth's sidereal rotation period is not a rational number, VSOP (u,v) coverages will not repeat after a certain number of orbits. Thus, the VSOP (u,v) coverage for a particular source improves with the number of orbits for which the source is observed. As noted in §5.2, for the highest resolution observations (in both dimensions) sources need to lie along or near either the orbit normal or orbit anti-normal direction. Under these circumstances there are relatively large holes in the (u,v) coverage that cannot be filled in by multi-orbit observations. Due to the relatively long time required to change source and the fact that the (u,v) coverage changes very rapidly near perigee, it is expected that VSOP observations will start at or near apogee and will continue for an integral number of orbits, except at the start of AO phase 1 observations when source changes will be scheduled during tracking station passes at Kagoshima. During this early phase of the mission it is important that source changes be monitored in real time from the only tracking station that can command the spacecraft. In a typical observing scenario it will require one orbit to change source and perform various spacecraft calibrations before observations, which will normally last 2, 3, or 4 orbits. One important observing constraint for the VSOP spacecraft is that only a maximum of 4 sources can be observed between daily commanding sessions from the Kagoshima Space Center.

9.10 Polarimetry

When obtaining VLBI polarization observations, one usually thinks in terms of a VLBI experiment in which all antennas record simultaneously both the left- and right-circularly-polarized (LCP and RCP) signals incident from a compact radio source. Information about the distribution of the total intensity and circularly polarized emission may be derived from the $L \otimes L$ and $R \otimes R$ ("parallel-hand") correlations. Information about the distribution of linearly polarized emission may be derived from the $R \otimes L$ and $L \otimes R$ ("cross-hand") correlations. Although the VSOP spacecraft will only receive one circular polarization (LCP), this does not imply that the VSOP spacecraft will be unable to participate in polarization observations. Essentially, only one of the two possible cross-hand correlations may be measured on the space-ground baselines, so that fewer visibility points would be available for construction of the polarization image; but useful polarization information would still be obtained. Roughly speaking, in order for a source's polarization to be detectable on baselines to the VSOP spacecraft, its compact polarized flux must exceed that baseline's detection limit.

One of the key issues connected with polarization observations is calibration of the antenna feed polarizations. For ground experiments, this has usually been done by making observations of a source of known (usually zero) polarization over a range of parallactic angles. Alternately, if one antenna polarization appearing in a given cross-hand correlation is known, the other may simply be solved for.

It is not feasible to frequently observe a polarization calibrator source with the VSOP spacecraft in order to obtain observations over a wide range of parallactic angles because this would entail an excessive amount of spacecraft slewing. The VSOP spacecraft is not free to rotate about the pointing direction, thus observations of a polarization calibrator source with the space-ground VLBI array while rotating the

spacecraft antenna about its pointing axis in order to measure the polarization properties of the antenna are also impossible.

The most straightforward approach to calibration of the VSOP spacecraft antenna polarization would be to use data on the ground-ground baselines to determine all instrumental polarization terms for all ground radio telescopes; then, remove these from the space-ground data, leaving only the instrumental contribution from the VSOP spacecraft antenna on these baselines. In this scheme, each space-ground baseline gives an independent estimate for the spacecraft polarization. This approach does not require a large number of spacecraft calibration observations taken over a range of parallactic angles, but rather simply 1 or 2 calibration observations, say, at the beginning and end of the set of observations on the target source(s). Information about the best polarization calibrator sources for VSOP polarization observations will come from ground-based VLBI polarization observations; the highest resolution ground-based VLBI polarization observations to date have been done at 1.3 cm, while observations at 7 mm will be attempted in the near future.

Problems in calibration of the VSOP spacecraft antenna polarization may arise if this polarization is significantly variable in a non-predictable way on the timescale of the observations on the target source(s). Such variations could be caused, for example, by changes in the shape of the antenna as it comes out of eclipse. Furthermore the polarization properties of the antenna are also expected to be a function of the angle between the source and the Sun. Very little information about the stability of the VSOP spacecraft antenna polarization is currently available; some information may potentially be obtained during the in-orbit checkout period.

The VSOP VLBA/MkIV/S2 compatible observing mode has two LCP 2-bit sampled 16-MHz channels. There are at least three ways in which polarization observations could be undertaken with the VSOP spacecraft. To obtain the maximum SNR for the spacecraft-ground polarized fringes the ground radio telescopes must observe with four (2 LCP, 2 RCP) 2-bit sampled 16-MHz channels which leads to a data rate of 256 Mbps. This data rate is twice the VLBA sustainable rate of 128 Mbps and can only be undertaken in exceptional circumstances. There are two observing modes that can be undertaken at the sustainable data rate of 128 Mbps. The first of these modes is for the ground radio telescopes to observe with two (1 LCP, 1 RCP) 2-bit sampled 16-MHz channels. This mode would result in a loss of polarized fringe sensitivity of a factor of $\sqrt{2} = 1.41$ compared to the maximum SNR mode. The second of these sustainable modes is for the ground radio telescopes to observe with four (2 LCP, 2 RCP) 1-bit sampled 16-MHz channels. This mode would result in a loss of polarized fringe sensitivity of only $\sqrt{0.88/0.64} = 1.17$ and is somewhat better than the first sustainable mode.

9.11 Spectral Line

The type of spectral line VLBI observations that may be conducted with the VSOP mission depend firstly on the properties of the VSOP spacecraft science subsystem, described in §3, and secondly on the properties of the correlator used to correlate the data. In this section we will assume the VSOP spacecraft is operating in the VLBA/MkIV/S2 compatible mode. In this mode the VSOP spacecraft has two 16-MHz channels and it is possible to independently set the frequency range of each of the two channels, provided that the lowest frequency in each channel is an integral number of MHz.

During AO phase 1 observations it is expected that most VSOP data will be correlated on either the NRAO VLBA correlator at Socorro or the NAO VSOP correlator at Mitaka. Table 12 compares the properties of these two correlators. For spectral line observers two important correlator properties are missing from this Table. The first is how many spectral channels are available per 16-MHz IF channel and the second is what is the correlation integration period. For the VLBA correlator each of the two 16-MHz channels can be resolved into 1024, 512, 256, 128, 64 or 32 spectral channels. Furthermore the output data from the VLBA correlator can be integrated over any integer multiple of the basic 131.072 milliseconds integration cycle with the restriction that the output data rate is limited to 0.5 Mbytes per second. The maximum velocity resolution with the VLBA correlator will be 0.2 $\mathrm{km\,s^{-1}}$ for H_2O masers and only 3 $\mathrm{km\,s^{-1}}$ for OH masers. The tracking stations used to track the VSOP spacecraft collect Doppler data which is used by spacecraft navigation teams in JPL and ISAS to determine the spacecraft orbit. This

orbit is then used by the relevant correlator during correlation. The estimated velocity error in this orbit is less than 4 mm s^{-1} (1 σ) for spacecraft altitudes above 5000 km but rises to 8.2 mm s^{-1} (1 σ) at 2500 km. With these velocity errors 22 GHz observations will always use the minimum 131.072 millisecond integration period. Linfield and Ellis (1994) have estimated that, for 10 station observations of water maser sources less than 1 arcsecond in extent, the output rate will be less than 0.3 Mbyte s^{-1} which is within the 0.5 Mbyte s^{-1} limit. For the VSOP correlator 8192 spectral lines channels per baseline are created and a maximum of 1024 spectral line channels can be output. These output channels can either be individual channels or combinations of channels from the 8192 channel data. Consequently the VSOP correlator can provide a factor of four higher spectral resolution compared to the VLBA correlator. Thus the velocity resolution with the VSOP correlator for H_2O and OH masers will be 0.053 km s^{-1} and 0.73 km s^{-1}. The minimum integration period of the VSOP correlator is 25 milliseconds and the maximum data output rate is 1.5 Mbyte s^{-1}.

10 Source Selection

It is up to the proposer to decide what to observe. However, to help the proposer in deciding what type of sources are observable with the VSOP mission the results of the Tracking and Data Relay Satellite System (TDRSS) space VLBI experiments conducted in the late 1980s, and the results of a recent 22 GHz VSOP pre-launch survey are presented in this section. The TDRSS results show there should be plenty of sources for VSOP to observe on baselines exceeding an Earth diameter, whereas the 22 GHz survey indicates which sources may be good candidates.

10.1 TDRSS Space VLBI Demonstrations

An element of the TDRSS was used for several space VLBI demonstrations between 1986 and 1988. Since the satellite had a geosynchronous orbit and a limited viewing region, only fringe-detection and very simple modelling could be performed. However, the success of the demonstrations, and the detection of fringes on baselines as long as 2.1 Earth diameters, showed that the space VLBI concept is technically feasible and that there are many radio sources with correlated flux densities and brightness temperatures high enough to be detected on baselines longer than an Earth diameter. Details of the TDRSS observations can be found in Levy *et al.* (1986), Levy *et al.* (1989), and Linfield *et al.* (1990).

The TDRSS space VLBI demonstrations provided valuable insight into the capability of space VLBI for detecting compact radio sources. The 4.9-meter TDRSS antenna had effective system temperatures of about 117,000 Jy at 2.3 GHz and 630,000 Jy at 15 GHz, with data rates of 28 Mbps and 176 Mbps, respectively. Therefore, given the VSOP spacecraft data rate of 128 Mbps, the 1.6- and 5-GHz sensitivities for a baseline to the VSOP spacecraft are about 6 times better than the sensitivity for a baseline from the same telescope to TDRSS at 2.3 GHz. At 22 GHz, the sensitivity for baselines to VSOP is expected to be about 4 times better than for a 15-GHz baseline from the same ground telescope to TDRSS.

Sources for the TDRSS experiments were selected based on the results of transcontinental VLBI surveys at 2.3 and 8.4 GHz that included the restricted declination range accessible to TDRSS. Candidates selected were the strongest compact objects with flat or inverted spectra and with high visibilities at 2.3 GHz and/or 8.4 GHz. In the experiment with the largest number of observed sources, 23 out of 24 sources were detected at 2.3 GHz on baselines as long as 2.1 Earth diameters (Linfield *et al.* 1989). Observed source brightness temperatures were $0.2\text{–}3.0\times10^{12}$ K, while co-moving brightness temperatures (in the source rest frames) were greater than 3×10^{12} K in several objects. Several other sources were detected in other experiments. Similar brightness temperatures were measured for the 11 (out of 22) sources detected at 15 GHz (Linfield *et al.* 1990), where the observations were hampered by a variety of technical problems. Therefore, long-baseline ground data should be a good predictor of which sources can be observed successfully with the VSOP spacecraft.

Table 10 provides a summary of both the 2.3-GHz TDRSS results, taken mostly from Linfield *et al.* (1989), and the 15-GHz TDRSS results, from Linfield *et al.* (1990). If it was possible to fit a Gaussian

model to the visibility data the observed brightness temperature is given in the final column of the table. Using this brightness temperature and Equation 10 the source size can be determined. In the TDRSS experiments several sources were found to be elliptical Gaussians and the source size determined from Equation 10 is therefore the square root of the geometrical product of the source major axis multiplied by the source minor axis.

10.2 22 GHz Pre-launch Continuum VLBI Survey

A 22 GHz pre-launch survey of 142 compact extragalactic radio sources on long Earth baselines has been conducted to enable potential sources for VSOP observations at this frequency to be identified (Moellenbrock *et al.* 1995, in preparation; Fujisawa 1995). These results fill a glaring void in the current literature and are presented in Table 11 (Moellenbrock and Fujisawa 1995, private communication). In addition to some correlated flux density data, an estimate of the *minimum* observed brightness temperature of the most compact component of each detected source is given. This quantity is determined by inverting Equation 11 to solve for T_b as follows:

$$T_b = 1.14 \times 10^{11} \left(\frac{S_c}{1\ Jy}\right)\left(\frac{D}{10^4\ km}\right)^2 \left(\frac{S_0/S_c}{\ln(S_0/S_c)}\right)\ \mathrm{K} \tag{22}$$

In this equation S_0 is the flux density of the most compact VLBI component in the source, which is assumed to be a circular Gaussian component. For a correlated flux density S_c on a baseline of projected length D, T_b has a minimum, T_b^{min}, when $S_0 = min(S_T, eS_c)$, where S_T is the total flux density of the source. T_b^{min} is strongly dependent on the baseline length and is therefore a much better constraint for the purposes of space VLBI planning when S_c is measured on the longest possible baseline. Note that an anomalously high value of S_c (due to fortuitous projected baseline length and orientation with respect to complex source structure) will inflate T_b^{min} artificially. Using T_b^{min}, S_0, and Equation 10 it is possible to work out an upper limit on the size of the most compact VLBI component.

Example: From the data in Table 11 and using Equation 11, the correlated flux of 0202+149 (with $S_0 = S_T = 2.89$ Jy) is expected to exceed 0.41 Jy on a baseline of 25,000 km. Using Equation 10, an upper limit on the size of the component of 0.08 mas is obtained.

11 VSOP Scheduling Process

11.1 How Does VSOP Differ from Other Space Astronomy Missions?

Unlike most space astronomy missions, the VSOP mission *requires* co-observing ground telescopes to obtain any useful scientific data. The space VLBI mission has obtained commitments of time from ground radio observatories. Unless these cover 100% of the possible VSOP observing time and all possible requests from proposers, they constitute another mission constraint which must be taken into account in the scheduling process.

11.2 What Ground Radio Telescopes Will be Available?

Table 8 lists the ground radio telescopes (GRTs) expected to support space VLBI observations along with their SEFD values at the VSOP observing frequencies (as expected in late 1996) and the percentage of the time that these telescopes have committed to space VLBI. All ten VLBA telescopes will be available as a single unit only. This will also be true of the EVN as a whole for 15% of the time (half the EVN network time), but some individual telescopes in the EVN will be available another 5–15% of the time. Each of the remaining telescopes in Table 8 has been committed only individually, but can be gathered into an *ad hoc* array depending on availability. Ground observatories which are not fully dedicated to VLBI, such as the EVN and ATNF telescopes, prefer time to be allocated in blocks. It should also be noted that some

Table 10: TDRSS Results at 2.3 GHz and 15 GHz

TDRSS Results at 2.3 GHz

Source Name	ID	z	Maximum Baseline ($D_\oplus$)	Total Flux (Jy)	Visibility on Max. Baseline	Model Flux (Jy)	Observed T_b (10^{12} K)
0048−097	BL	···	1.50	0.9	0.63	0.62	>1.25
0229+131	Q	2.059	1.19	1.9	0.37		
0336−019	Q	0.852	1.37	1.8	0.50	1.52	>1.10
0414−189	Q	1.536	1.65	0.6	0.70		
0420−014	Q	0.915	1.38	3.6	0.63	3.43	>1.64
0434−188	Q	2.702	1.59	0.9	0.46		
0454−234	Q	1.003	1.81	1.6	0.16		
0723−008	N	0.128	1.31	1.9	0.16	1.07	0.22
0727−115	Q	···	1.56	3.9	0.12	3.90	1.28
0805−077	Q	1.837	1.18	1.1	0.45		
0823+033	BL	0.506	1.18	1.2	0.20		
1034−293	BL	0.312	2.15	1.0	0.29	0.58	0.70
1124−186	Q	1.050	1.60	0.8	0.36		
1127−145	Q	1.187	1.64	5.0	0.08		
1145−071	Q	1.345	1.35	0.8	0.26		
3C 273	Q	0.158	1.14	36.0	0.03		
3C 279	Q	0.538	1.35	10.3	0.33	6.82	1.03
1334−127	Q	0.541	1.69	3.1	0.15	2.21	>0.82
1504−166	Q	0.876	1.70	3.0	0.31		
1510−089	Q	0.360	1.22	0.8	0.41		
1519−273	BL	···	2.02	1.6	0.66	1.59	2.94
1730−130	Q	0.902	1.40	1.8	0.17		
1741−038	Q	1.054	1.47	2.1	0.31	2.11	0.45
1921−293	Q	0.352	2.07	8.6	0.15	3.49	2.81
1958−179	Q	0.650	1.44	1.6	0.64	1.65	1.47
2216−038	Q	0.901	1.23	2.6	0.51	1.78	>1.68
3C 446	Q	1.406	0.94	5.2	0.09		
2345−167	Q	0.576	1.67	2.1	0.17	1.27	>0.62
0221+067	Q	0.511	1.12	0.9	<0.5		
2131−021	Q	0.557	0.67	1.3	<0.20		
2318+049	Q	0.622	1.22	1.2	<0.4		

TDRSS Results at 15 GHz

Source Name	ID	z	Maximum Baseline ($D_\oplus$)	Total Flux (Jy)	Visibility on Max. Baseline	Model Flux (Jy)	Observed T_b (10^{12} K)
0221+067	Q	0.511	1.32	1.5	0.52		
0727−115	Q	···	1.35	4.0	0.18	1.89	0.54
0823+033	BL	0.506	1.26	1.4	0.51	0.66	0.50
1055−018	Q	0.888	0.86	3.6	0.43		
3C 273	Q	0.158	1.33	20.0	0.07	3.49	0.98
3C 279	Q	0.538	1.40	8.4	0.16	4.84	1.29
1334−127	Q	0.539	1.63	3.8	0.37	2.87	1.47
1510−089	Q	0.360	1.18	2.3	0.57	2.76	1.14
1730−130	Q	0.902	1.14	4.1	0.18	1.88	0.46
2145+067	Q	0.990	1.38	6.3	0.20	5.43	1.17
3C 446	Q	1.404	1.49	5.1	0.23	1.98	1.00
0229+131	Q	2.059	1.50	1.6	<0.4		
1127−145	Q	1.187	1.13	1.6	<0.8		
1244−255	Q	0.638	1.46	0.9	≤1.0		
1519−273	BL	···	1.57	1.2	≤1.0		
1749+096	Q	0.322	1.28	1.4	<0.9		
1921−293	Q	0.352	1.52	5.5	<0.3		
2121+053	Q	1.878	1.21	1.5	<0.9		
2216−038	Q	0.901	1.19	···	≤1.0		
2230+114	Q	1.037	1.22	···	≤1.0		
2318+049	Q	0.622	1.47	1.3	<0.5		
2345−167	Q	0.576	1.59	1.6	<0.4		

Table 11: 22 GHz Continuum Pre-Launch Survey (10 August 1995 Version)

SOURCE NAME		z	Type	Total Flux (Jy)	MAXIMUM CORRELATED FLUX: Correlated Flux (Jy)	Error	Projected Baseline (10^4 km)	MAXIMUM BASELINE: Correlated Flux (Jy)	Error	Projected Baseline (10^4 km)	MINIMUM T_b (10^{12} K)	Error
0007+106	IIIZW2	0.090	G	0.44	0.34	0.03	0.7264	0.34	0.03	0.7264	0.103	0.040
0016+731		1.781	Q		0.17	0.03	0.3195	0.15	0.02	0.3249	0.005	0.001
0048−097			BL	2.05	1.53	0.24	0.2118	0.70	0.08	1.0705	0.249	0.028
0106+013	OC012	2.107	Q	3.04	1.57	0.25	1.0329	1.50	0.24	1.0589	0.550	0.139
0112−017		1.365	Q	1.08	0.81	0.13	0.2629	0.39	0.05	1.0811	0.141	0.018
0119+041		0.637	Q	1.41	0.56	0.08	0.7460	0.37	0.06	1.0579	0.128	0.021
0119+115		0.570	Q		1.12	0.19	0.5683	0.69	0.07	0.7398	0.117	0.012
0122−003		1.070	Q		0.63	0.10	0.2723	0.48	0.07	0.3539	0.019	0.003
0133+476	DA55	0.859	Q		1.93	0.30	0.4376	1.66	0.16	0.7301	0.274	0.026
0149+218		1.320	Q		0.84	0.08	0.7201	0.77	0.08	0.7291	0.127	0.013
0202+149			Q	2.89	2.04	0.33	1.0554	2.04	0.33	1.0554	1.054	0.585
0202−172		1.740	Q		0.38	0.05	1.0755	0.38	0.05	1.0755	0.136	0.018
0212+735		2.367	Q		1.31	0.21	0.2855	1.31	0.20	0.2895	0.034	0.005
0221+067		0.511	Q		1.05	0.15	0.7458	0.77	0.12	1.0551	0.266	0.041
0224+671	4C67.05		Q		1.24	0.20	0.2531	1.16	0.19	0.2593	0.024	0.004
0229+131		2.065	Q	1.31	0.68	0.10	0.7377	0.48	0.08	1.0589	0.167	0.028
0234+285	CTD20	1.207	Q	2.79	2.54	0.40	1.0196	1.62	0.26	1.0587	0.656	0.214
0235+164	OD160	0.940	BL	4.35	3.44	0.55	1.0422	2.53	0.41	1.0589	1.026	0.339
0237−027		1.116	Q		0.85	0.13	0.3286	0.46	0.05	1.0287	0.151	0.016
0300+470	OE400		BL	5.89	0.69	0.07	0.6377	0.48	0.05	0.7350	0.080	0.008
0316+413	3C84	0.017	BL	25.80	1.62	0.24	0.9915	0.57	0.09	1.0509	0.195	0.031
0333+321	NRAO140	1.259	Q	1.93	2.02	0.31	1.0036	1.60	0.26	1.0579	1.313	2.998
0336−019	CTA26	0.852	Q	3.37	2.08	0.33	0.3164	0.46	0.06	1.0667	0.162	0.021
0402−362		1.417	Q	2.71	0.41	0.15	0.6175	0.41	0.15	0.6175	0.048	0.018
0403−132		0.571	Q	2.24	0.83	0.07	0.7301	0.62	0.07	1.0597	0.216	0.024
0420−014		0.915	Q	3.90	2.13	0.31	0.2528	1.66	0.20	1.0761	0.603	0.105
0422−380		0.782	Q		0.29	0.11	0.5944	0.29	0.11	0.5944	0.032	0.012
0426−380		1.030	BL		0.11	0.04	0.5956	0.11	0.04	0.5956	0.012	0.004
0430+052	3C120	0.033	G	2.24	0.48	0.07	0.7458	0.10	0.02	1.0548	0.034	0.007
0454−234	OF-292	1.003	Q		1.06	0.13	0.9924	1.06	0.13	0.9924	0.324	0.040
0458−020		2.286	Q		0.83	0.10	1.0803	0.83	0.10	1.0803	0.300	0.036
0528+134		2.070	Q	6.31	5.36	0.78	0.3710	3.69	0.46	1.0795	1.562	0.406
0552+398	DA193	2.365	Q	5.86	1.93	0.28	0.4287	0.39	0.04	0.7333	0.065	0.007
0605−085		0.872	Q	2.67	2.24	0.33	0.3240	1.80	0.23	1.0722	0.888	0.321
0642+449	OH471	3.406	Q	2.11	1.64	0.28	1.0582	1.64	0.28	1.0582	1.069	1.126
0710+439	OI417	0.518	G		< 0.19	0.04	0.5875					
0723−008		0.127	BL		0.52	0.08	0.3641	0.42	0.04	0.7221	0.068	0.006
0727−115				4.64	0.76	0.27	0.7392	0.46	0.06	1.0583	0.160	0.021
0735+178	DA237	0.424	BL	2.22	0.51	0.08	0.7305	0.29	0.05	1.0574	0.101	0.017
0736+017	OI061	0.191	Q		0.65	0.12	1.0241	0.34	0.06	1.0583	0.118	0.021
0738+313	OI363	0.630	Q		0.33	0.05	0.6144	0.23	0.04	0.6235	0.028	0.005
0745+241		0.409	Q		0.65	0.10	0.3983	0.36	0.04	0.7402	0.061	0.007
0748+126		0.889	Q		1.23	0.19	0.8200	0.07	0.01	1.0577	0.024	0.003
0754+100	OI090.4	0.660	BL	1.51	1.11	0.17	0.7985	0.33	0.06	1.0570	0.114	0.021
0804+499		1.433	Q		0.55	0.08	0.4387	0.48	0.05	0.6709	0.067	0.007
0808+019			BL	1.55	1.45	0.23	0.8068	0.47	0.06	1.0670	0.166	0.021
0814+425	OJ425	0.258	BL		0.46	0.07	0.4307	0.21	0.02	0.7056	0.032	0.003
0823+033		0.506	BL	1.53	1.14	0.18	0.8109	0.37	0.06	1.0550	0.128	0.021
0823−223		0.910	BL		< 0.09	0.02	0.6641					
0826−373					0.26	0.10	0.6142	0.26	0.10	0.6142	0.030	0.012
0851+202	OJ287	0.306	BL	2.76	1.61	0.25	0.3651	0.75	0.13	1.0562	0.259	0.045
0859−140		1.335	Q		0.13	0.02	0.7069	0.13	0.02	0.7069	0.020	0.003
0917+449		2.180	Q	2.05	1.15	0.18	0.4352	1.02	0.10	0.7348	0.181	0.031
0919−260	OK-232	2.300	Q	1.12	0.23	0.09	0.6804	0.23	0.09	0.6804	0.033	0.013
0920−397		0.591	Q		0.09	0.03	0.5715	0.09	0.03	0.5715	0.009	0.003
0923+392	4C39.25	0.699	Q	10.30	2.71	0.43	0.4251	0.71	0.12	1.0586	0.247	0.042
0945+408		1.252	Q		< 0.20	0.03	0.7379					
0953+254	OK290	0.712	Q		0.33	0.05	0.6965	0.22	0.03	0.7024	0.034	0.005
1012+232		0.565	Q	0.90	0.43	0.06	0.7135	0.43	0.06	0.7135	0.071	0.015
1034−293		0.312	Q	1.90	1.16	0.14	1.0194	1.16	0.14	1.0194	0.456	0.124
1045−188		0.595	Q		0.90	0.11	1.0327	0.90	0.11	1.0327	0.298	0.036
1055+018	OL093	0.888	Q	3.41	1.46	0.25	1.0520	1.46	0.25	1.0520	0.507	0.116
1116+128		2.118	Q	1.41	0.62	0.10	0.5521	0.61	0.10	0.6289	0.076	0.017
1124−186					1.10	0.13	1.0574	1.10	0.13	1.0574	0.381	0.045
1144+402		1.089	Q	1.39	0.86	0.08	0.6670	0.77	0.07	0.7167	0.138	0.026
1150+812		1.250	Q		0.92	0.14	0.3821	0.92	0.14	0.3821	0.042	0.006
1156+295	4C29.45	0.729	Q	1.37	1.26	0.20	0.9925	0.63	0.10	1.0385	0.217	0.050
1213−172				1.62	0.84	0.13	0.6874	0.52	0.18	0.7148	0.082	0.029
1219+285	ON231	0.102	BL	0.61	0.17	0.03	0.8042	0.10	0.02	1.0569	0.035	0.007
1226+023	3C273B	0.158	Q	33.40	7.79	1.20	0.3244	1.13	0.19	1.0587	0.393	0.066
1228+126	3C274	0.004	G		0.49	0.04	0.6461	0.17	0.02	1.0803	0.062	0.007
1244−255		0.638	Q	1.48	0.93	0.12	1.0786	0.93	0.12	1.0786	0.422	0.130
1253−055	3C279	0.538	Q	17.40	11.64	1.80	0.2230	5.70	0.71	1.0799	2.061	0.257
1308+326	OP313	0.997	Q	1.44	2.36	0.39	1.0373	2.36	0.39	1.0373	0.787	0.130
1334−127		0.539	Q	6.44	4.59	0.55	0.9855	4.59	0.55	0.9855	2.106	0.843

Table 11: 22 GHz Continuum Pre-Launch Survey (10 August 1995 Version) *continued*

SOURCE NAME		z	Type	Total Flux (Jy)	MAXIMUM CORRELATED FLUX: Correlated Flux (Jy)	Error	Projected Baseline (10^4km)	MAXIMUM BASELINE: Correlated Flux (Jy)	Error	Projected Baseline (10^4km)	MINIMUM T_b (10^{12}K)	Error
1354+195		0.719	Q	1.06	0.71	0.12	1.0044	0.14	0.02	1.0587	0.049	0.007
1413+135		0.247	BL	0.45	0.18	0.03	0.8208	0.15	0.02	1.0519	0.051	0.007
1418+546	OQ530	0.152	BL		0.35	0.05	0.4395	0.35	0.05	0.4395	0.021	0.003
1435+638		2.062	Q		< 0.31	0.05	0.6939					
1502+106	OR103	1.833	Q	1.28	1.19	0.19	0.9822	0.07	0.01	1.0582	0.024	0.003
1504+377	OR306	0.674	G	1.19	0.82	0.13	0.4228	0.60	0.06	0.7404	0.109	0.019
1504−166		0.876	Q	2.04	0.64	0.08	1.0435	0.58	0.07	1.0796	0.210	0.025
1510−089		0.360	Q	2.80	1.68	0.26	0.2246	1.28	0.17	1.0799	0.476	0.095
1514−241		0.048	BL		0.42	0.05	1.0737	0.42	0.05	1.0737	0.150	0.018
1546+027		0.412	Q	3.10	2.95	0.44	0.8166	0.79	0.10	1.0810	0.286	0.036
1548+056		1.422	Q	1.64	0.99	0.16	0.2989	0.54	0.07	1.0598	0.188	0.024
1606+106		1.226	Q	0.98	0.75	0.12	0.3539	0.38	0.04	0.7400	0.065	0.010
1611+343	DA406	1.401	Q	3.06	3.80	0.58	0.9764	2.86	0.46	1.0508	5.698	3.205
1633+382	4C38.41	1.814	Q	1.72	1.34	0.21	1.0354	1.31	0.21	1.0496	0.793	0.637
1637+574	OS562	0.745	Q	1.97	0.74	0.11	0.4390	0.42	0.04	0.6733	0.059	0.006
1638+398	NRAO512	1.666	Q	1.48	3.07	0.48	0.9993	2.28	0.36	1.0497	0.779	0.123
1641+399	3C345	0.594	Q	9.47	10.65	1.51	0.6129	2.27	0.36	1.0507	0.777	0.123
1642+690		0.749	G	1.47	0.30	0.03	0.7110	0.25	0.02	0.7143	0.040	0.003
1652+398	DA426	0.033	BL	1.04	0.29	0.05	0.4270	0.22	0.02	0.7345	0.037	0.003
1655+077	OS092	0.621	Q	1.14	0.75	0.12	1.0149	0.63	0.11	1.0577	0.245	0.079
1656+477		1.622	Q		0.26	0.04	0.5591	0.21	0.02	0.7375	0.035	0.003
1716+686		0.777	Q		0.22	0.02	0.7160	0.22	0.02	0.7160	0.035	0.003
1730−130	NRAO530	0.902	Q	5.62	2.55	0.40	0.8080	2.11	0.26	1.0585	0.733	0.118
1739+522	OT566	1.379	Q		1.84	0.28	0.4398	1.15	0.11	0.6652	0.158	0.015
1741−038		1.057	Q	3.65	2.67	0.42	0.3455	1.81	0.24	1.0811	0.693	0.150
1749+096	OT081	0.320	Q	3.51	3.80	0.55	0.7793	2.50	0.41	1.0513	1.303	0.764
1758+388	OT398	2.092	Q		0.46	0.08	0.6250	0.29	0.03	0.7412	0.049	0.005
1800+440	OV401	0.663	Q		1.19	0.17	0.5755	0.88	0.14	1.0582	0.305	0.049
1803+784		0.684	BL	2.23	1.13	0.18	0.3968	0.97	0.09	0.7288	0.162	0.024
1807+698	3C371	0.051	BL	1.75	0.43	0.04	0.7148	0.22	0.02	0.7210	0.035	0.003
1823+568		0.664	BL	2.87	1.47	0.23	0.4379	1.19	0.12	0.6970	0.181	0.028
1828+487	3C380	0.692	Q		0.62	0.10	0.4395	0.62	0.10	0.4395	0.037	0.006
1849+670		0.657	Q		0.54	0.05	0.7118	0.52	0.05	0.7224	0.084	0.008
1901+319	3C395	0.635	Q	1.25	0.70	0.11	0.4077	0.48	0.05	0.6924	0.071	0.011
1908−201	OV-213			2.58	0.89	0.14	0.6723	0.76	0.09	1.0473	0.258	0.031
1921−293	OV-236	0.352	BL	17.30	12.56	1.56	1.0664	12.56	1.56	1.0664	7.005	3.124
1923+210	OV239.7			2.12	1.79	0.27	0.9665	1.24	0.20	1.0579	0.504	0.168
1928+738	4C73.18	0.303	Q	3.15	1.19	0.19	0.3903	0.83	0.08	0.7292	0.137	0.013
1936−155		1.657	Q		0.70	0.09	1.0686	0.70	0.09	1.0686	0.248	0.032
1954+513	OV591	1.230	Q	2.30	1.43	0.22	0.4245	1.01	0.09	0.7011	0.157	0.023
2005+403		1.736	Q	2.76	2.89	0.41	0.6091	0.20	0.03	1.0490	0.068	0.010
2007+777		0.342	BL	1.72	0.60	0.06	0.7299	0.60	0.06	0.7299	0.099	0.010
2008−159		1.180	Q		0.53	0.09	0.8019	0.38	0.05	1.0767	0.137	0.018
2021+317				2.17	0.42	0.06	0.6710	0.31	0.05	1.0583	0.108	0.017
2021+614	OW637	0.227	G	2.46	0.89	0.14	0.4000	0.33	0.03	0.7257	0.054	0.005
2022+542	OW538				< 0.29	0.05	0.6892					
2059+034		1.015	Q	2.26	1.68	0.26	0.3774	1.44	0.19	1.0606	0.643	0.209
2121+053	OX036	1.941	Q		0.59	0.06	0.6752	0.49	0.06	1.0749	0.176	0.021
2128−123		0.501	Q	2.02	0.23	0.04	0.8064	0.12	0.01	1.0426	0.040	0.003
2134+004	OX057	1.936	Q	5.03	0.54	0.08	0.7425	0.35	0.06	1.0569	0.121	0.021
2136+141	OX161	2.427	Q	2.00	0.91	0.14	0.9652	0.62	0.10	1.0519	0.213	0.034
2145+067	DA562	0.999	Q	8.91	5.97	0.93	0.3596	1.60	0.20	1.0742	0.572	0.072
2155−152	OX-192	0.672	Q	2.26	0.34	0.05	1.0742	0.29	0.04	1.0811	0.105	0.014
2200+420	BLLAC	0.069	BL	1.63	2.74	0.38	0.5834	0.67	0.11	1.0589	0.234	0.050
2201+315	4C31.63	0.298	Q	2.16	0.88	0.13	0.8209	0.18	0.03	1.0586	0.063	0.010
2203−188		0.619	Q	1.77	< 0.14	0.03	1.0806					
2216−038		0.901	Q	1.82	0.76	0.13	0.5484	0.75	0.24	0.7456	0.130	0.051
2223−052	3C446	1.404	Q	3.67	2.18	0.71	0.7460	0.37	0.04	0.9932	0.113	0.012
2227−088		1.562	Q	1.07	1.18	0.15	1.0744	1.18	0.15	1.0744	0.422	0.054
2230+114	CTA102	1.037	Q	2.63	1.62	0.25	1.0024	1.18	0.19	1.0583	0.419	0.095
2234+282		0.795	Q		0.73	0.11	0.6632	0.22	0.04	1.0587	0.076	0.014
2243−123	OY-172.6	0.630	Q	2.65	0.78	0.13	0.8060	0.43	0.05	1.0760	0.154	0.018
2251+158	3C454.3	0.859	Q	11.70	7.46	1.17	0.3542	2.44	0.39	1.0554	0.842	0.135
2255−282		0.926	Q	2.66	0.57	0.19	0.6874	0.52	0.07	1.0804	0.188	0.025
2318+049		0.623	Q	0.62	0.52	0.05	0.7154	0.52	0.05	0.7154	0.206	0.151
2351+456	OZ486	1.992	Q	1.02	0.43	0.07	0.4356	0.41	0.04	0.6148	0.048	0.007
2355−106		1.622	Q		0.26	0.05	0.7922	0.18	0.02	1.0397	0.060	0.007

Type: Q = quasar, G = galaxy, BL = BL Lac object.

observatories have especially high programme pressure at certain times of year, e.g. Effelsberg during night time in May through July when Galactic Center observations may take preference. For a discussion of the different VSOP observational programs please consult the VSOP Announcement of Opportunity §3.

11.3 How Will VSOP and Ground VLBI Scheduling Differ ?

The scheduling of VLBI experiments with the VSOP mission will be performed by the VSOG. Unlike ground VLBI experiments, the (u,v) coverage attainable for a particular source can vary greatly with time. Because of the large solar avoidance angle and the telemetry antenna horizon mask, certain regions of the sky are unobservable for periods of up to 5 months. Even when a source is observable, because of the orbital precession, the (u,v) coverage attainable could be somewhat foreshortened or even one-dimensional at certain times. This may or may not be acceptable for a particular science program.

To find the best period in which to observe a source the scheduler must search over many possible observing slots — 17 months for AO phase 1 observations — to determine when the preferred (u,v) coverage occurs. Performing this for each source in each program results in having to schedule many hundreds of observations for each AO phase. In this process a proposer may not receive the preferred (u,v) coverage (see below for more details).

11.4 How Will the Scheduling Process Work?

As with most other open-proposal observatories, whether or not an observing program "wins" is determined by the scientific value of the program and the availability of the resources it requires. The first step in this process will be an evaluation of each proposal by an independent and international Science Review Committee (SRC). In addition, in consultation with a technical review by the VSOG, the SRC may recommend an increase or decrease in the amount of observing time and ground facilities an observation needs to accomplish its stated scientific goals. After the evaluation process is complete, the VSOG will then begin to schedule observations in proposal ranking order (highest ranked proposals first) until all the available resources are used up. Some amount of schedule shifting will be employed to allow as many highly-ranked programs as possible to be scheduled. This may result in many programs having (u,v) coverage that is not as good as the proposer desires in the effort to optimally allocate all the highly rated scientific programs. The result of this effort will be a "long-term" schedule over the entire AO phase 1 observing period. It will be used to periodically generate "detailed" schedules of a few weeks in duration.

A major re-generation of the long-term schedule may be necessary after launch when the actual VSOP spacecraft orbital elements are known. Additional re-generations may be necessary, if the spacecraft or mission capabilities change, especially as the AO phase 1 observing proceeds.

11.5 How Many GRTs do I Ask for ?

During the schedule creation phase, in order that a program is not prematurely dropped from consideration, it will be *imperative* for the scheduler to know the *minimum* amount of resources that a program needs to accomplish most of its goals. The 'Ground Radio Telescopes' item on the VSOP proposal Cover Sheets should be filled in with both the 'Preferred choice' array *and* with the 'Minimum acceptable:' array. Initially, the scheduler will make an attempt to schedule the 'Preferred choice' array. If that is unsuccessful (*e.g.*, if all requested resources have been used up by previously-scheduled, more highly-rated, programs), then the 'Minimum acceptable' array will be attempted. If even the 'Minimum acceptable' array is not available, then an observation will not be scheduled at all.

Note that, once an observation is scheduled in a particular time slot, that observation will have the use of *all* the ground radio telescopes committed to space VLBI observations at that time. This often will be more than the 'Minimum acceptable' array. This can be done because (1) ground radio telescopes

usually are committed in blocks of time — often in arrays as well — and (2) during the AO phase 1 observing period, there will be only one space VLBI mission competing for those resources.

With this method of allocating resources, there is a good chance of getting the 'Preferred choice' array if a proposal has high scientific value. On the other hand, if it is not ranked as highly, a proposal can maximize its chances of "winning" by having the 'Minimum acceptable' array as small as possible but still able to accomplish some or most of its scientific goals. As long as the 'Minimum acceptable' array is scientifically sound, a program is not penalized by keeping this array as small as possible.

11.6 How Does the Proposer Interface with the Scheduling Process?

Because the scheduling process is complex, the scheduler will have little time for detailed and frequent interactions with the proposers. Personal or e-mail interactions usually will be scheduler-initiated. The first and foremost interaction with the scheduler will be through the proposal Cover Sheets. These have been designed to give the proposer some ability to control the scheduling process before it begins. Some of the crucial items are the preferred GRT array (discussed above), desired length of observation, preferred range of observing dates, desired (u,v) coverage type and position angle, and, for monitoring programs, the preferred number of observations and their mean interval spacing and range.

Once the long-term schedule has been generated, the PI (or designated contact person) will be notified by the VSOG of the tentative date(s) on which their observation(s) has (have) been tentatively scheduled. If this is significantly in the future, there is a chance that the scheduled date may change in the intervening time. Once a firm observing date has been determined, the PI will again be notified by the VSOG. It is at this stage that the PI may become involved in the detailed scheduling of the observation, if they have so requested to do so on item (9) of the proposal Cover Sheets.

Once a detailed schedule for the observation has been created and a firm observing date determined, the PI will again be notified by the VSOG.

If at any time information on the Cover Sheets changes between writing the proposal and scheduling the observation (*e.g.*, the date of simultaneous observation with optical or X-ray telescopes), these facts must be transmitted immediately to the VSOG by e-mail (vsog@vsop.isas.ac.jp).

12 Space VLBI Data Correlation

12.1 Correlators

Table 12: Correlator Properties

Correlator	Location	Stations	Format	Operational	Copiers
VLBA	Socorro, NM, USA	20	VLBA/MkIV	1994	None
VSOP	Mitaka, Japan	10	VSOP	1995	$2 \times$ (VLBA $\rightarrow$ VSOP) $1 \times$ (S2 $\rightarrow$ VSOP)
EVN/JIVE	Dwingeloo, Netherlands	16	MkIV/VLBA	1997	None

A comparison of the correlators that are able to support correlation of VSOP data is shown in Table 12. VLBI data collected on the VLBA and MkIV recording systems can be correlated at either the VLBA correlator or the Joint Institute for VLBI in Europe (JIVE) correlator, which is due to come on-line in late 1997. All the VLBI data acquisition tracking stations have VLBA recorders. The Usuda station also has a VSOP recorder. In general, NRAO has committed the VLBA correlator to processing experiments involving NRAO telescopes, including the VLBA, the VLA, and the Green Bank 43m. The VLBA correlator has a 20 station capability but no tape-copy facilities. The remainder of the observations will be correlated either by the VSOP correlator or by the JIVE correlator. The VSOP correlator at

the National Astronomical Observatory (NAO) in Mitaka has the capability of processing 10 observing stations using VSOP recorders in a single pass. Tape copiers at Mitaka will be available to copy data from VLBA and S2 tapes to VSOP tapes. The Joint Institute for VLBI in Europe (JIVE) is building a 16 station MkIV correlator. This correlator is due to become operational in late 1997, and probably will be used to correlate many VSOP experiments involving the EVN. Note that with the exception of VLBI data recorded on the VLBA and MkIV systems, experiments involving two or more recording systems will require tape-copying at Mitaka before correlation and must be correlated at Mitaka. Thus any experiment using non-VLBA/MkIV recorders will at least require tape translation of the VLBI data recorded at four of the five tracking stations and must be correlated at Mitaka.

There is no requirement for proposers to be present during correlation.

12.2 Correlator Output

The PI will be sent the correlated data and necessary calibration files in the standard format that is used by present day ground VLBI. Present practice is to distribute the correlated data on either Exabyte or DAT tape in FITS format. It is expected that experiments will be correlated in less than 60 days after the experiment takes place since there is a finite tape pool and tapes must be recycled in a timely fashion. After correlation has been judged complete and correct at a correlator, the tapes will be erased and re-used. The PI will have no option to ask that the raw tapes be kept until final data analysis is complete.

13 VSOP Spacecraft Data Calibration

Proposers need to be aware of the general VLBI calibration scheme for the VSOP spacecraft. There are three main types of calibration measurements that need to be performed:

- Measurement of the antenna gain.
- Measurement of the system temperature.
- Measurement of the phase difference between the two VSOP channels.

Once the antenna gain and the system temperature are measured for each antenna participating in a VLBI experiment it is then possible to calibrate the amplitudes of the VLBI visibility data.

13.1 Antenna Gain

In order to calibrate VLBI data the gain of each antenna must be measured for each observing band. For a ground antenna the gain is normally a function of only the source elevation; thus for ground antennas the gain–elevation curve needs to be measured. For a space antenna, such as the VSOP spacecraft, there is an analog to the gain-elevation curve. This is the gain–Sun-angle curve, where the Sun-angle is the angle between the source and the Sun. Furthermore the satellite will undergo eclipses of variable length and it is expected for a given Sun angle that the antenna gain will also be a function of both the eclipse length and the time since the last eclipse. The VSOP spacecraft antenna gain will be measured periodically as a function of both Sun angle and eclipse history by boresight calibration using water masers at 22 GHz and OH masers at 1.6 GHz. At 5 GHz the gain will be measured using continuum radio sources and a near real time VLBI correlator at Usuda. It is NOT the responsibility of the proposers to measure the antenna gain – this activity will be undertaken by the VSOG.

13.2 System Temperature

Unlike many ground radio telescopes, the VSOP satellite does NOT have the ability to measure system temperature continuously. Due to the limited on-board spacecraft command memory it will only be

possible to measure the system temperature on average every $\approx$ 10 minutes. This is achieved by switching on a noise diode for 7 seconds and injecting the noise diode signal at a 4 Hz rate into the LNA. The noise diode will approximately double the system temperature, so in a typical 7 second measurement period the error in the system temperature measurement will be 0.1% in a 16 MHz channel. The VSOP spacecraft system temperature is expected to be primarily a function of the physical temperature of various science subsystem components. The maximum temperature variations will occur when the spacecraft comes out of eclipse. However near perigee the presence of the Earth in the main antenna sidelobes is expected to add a significant amount (up to 60 K) to the antenna temperature (Murphy 1994). Near perigee and when the VSOP spacecraft is coming out of eclipse the system temperature will be measured more frequently.

It will be the responsibility of the VSOG and not the PI to determine and implement the calibration scheme for a particular observation. Any non-standard requirements of a particular experiment *must* be specified in the proposal Cover Sheets and justified in the technical and scientific justification.

13.3 Channel Phase Differences

In two of the three VSOP observing modes, including the mode that is VLBA/MkIV/S2 compatible, two channels of VLBI data are recorded. There is however an arbitrary phase offset between these two channels which is expected to vary slowly with time. This phase difference needs to be measured and removed from the VLBI data if the two channels are to be coherently averaged. To measure this phase difference a series of phase calibration tones can be continuously injected into the LNAs at 1 MHz intervals. The sum of the power in these tones is only 0.4% of the system temperature power. These tones will be extracted and used to align the two channels. This alignment of the channels can take place either when the data is correlated or after correlation. The PI of an experiment will not have to worry about the extraction of these tones as these details will be taken care of by the VSOG, with results reported to the proposer in FITS tables accompanying the correlator output data. By default, for continuum observations the tones will always be on and for spectral line observations they will always be off. The phase cal tones are also used for bandpass calibration within each channel.

13.4 Summary

From the above three subsections it can be seen that the VSOG is responsible for developing the calibration scheme for the VSOP spacecraft. The VSOG will generate a spacecraft log file that contains all the relevant information to calibrate data from the VSOP spacecraft. This file will be in a standard format so that the usual programs used for calibrating VLBI data can be used, such as the ANCAL program in AIPS.

14 VSOP Proposal Aid Software

As has been demonstrated in several sections of this guide, observing with the VSOP spacecraft will be different from what is normally encountered with ground VLBI. To help potential users better understand the VSOP mission and hence write better proposals, three sets of software have been written to enable proposers to plan experiments. The major difference between the three software packages is the platforms they run on and what functions they can perform. Software inter-comparisons have shown that the three sets of software give the same correct results for the functions they have in common. Table 13 compares the three software packages. Further details on the individual packages are provided in the following subsections.

14.1 FAKESAT

The JPL Space VLBI Project has developed a space VLBI simulation program, called FAKESAT, that enables proposers to the space VLBI missions, VSOP and RadioAstron, plan their experiments. FAKE-

Table 13: Comparison of the JPL, Calgary and SGO SVLBI Proposal Aid Packages

Package	FAKESAT	SPAS	SVPIS
Organization	JPL	SGO	U. of Calgary
Country	USA	Hungary	Canada
Platform	UNIX	PC	PC
Feature			
VSOP spacecraft constraints	•	•	•
Satellite ground track	•	•	•
(u,v) plot	•	•	•
All-Sky (u,v) plot	•		•
(u,v) plot as a function of time	•		
Rotating Earth movie	•	•	
Create simulated data	•		•
Radio telescope timeline	•	•	•
SNR calculations	•	•	•
Polarization simulations			•

•= software package supports this feature
SPAS = Space VLBI Assistance Software
SVPIS = Space VLBI Principal Investigator Software
SGO = Satellite Geodetic Observatory

SAT was derived from the well-established Caltech VLBI package program FAKE and has a mouse-driven, interactive point and click, X-windows interface. At present FAKESAT runs on Sun and HP workstations but it should be easy to port it to other UNIX platforms. It requires the Caltech PGPLOT library. A variety of VSOP simulations can be undertaken with FAKESAT (see Table 13).

FAKESAT is available either from the JPL SVLBI Project WWW site (http://sgra.jpl.nasa.gov) or by anonymous ftp from sgra.jpl.nasa.gov (128.149.70.4) with the relevant compressed tar and README files in the pub/software/fakesat directory.

14.2 SPAS

The Space VLBI Assistance Software (SPAS) has been developed at the FÖMI Satellite Geodetic Observatory, Penc (Hungary). Some of the main functions of the software are shown in Table 13. A graphical user interface enables the user to communicate with the software as easily as possible. Commands can be given by mouse or keyboard. Plots and tables can be printed out on various printers. The recommended hardware (IBM PC/AT compatible) configuration is the following: MS-DOS or DR-DOS V5.0, V6.0, 80386 DX-33MHz processor with a 80387 co-processor, about 2MB free disk space, 4 MB RAM, SVGA with 1MB VRAM graphics card, keyboard + mouse input and a HP LaserJet printer.

The first version and the full user documentation is available on request. SPAS can be obtained by anonymous ftp from novell.sgo.fomi.hu (193.224.183.126) and is in the SPAS/EXE directory. For more information contact the project leader:

I. Fejes, FÖMI Satellite Geodetic Observatory, Penc, Hungary.
Postal address: H-1373 Budapest, P.O. Box 546.
Tel.: +36 27 310 980, fax: +36 27 310 982.
E-mail: vlbi_group@novell.sgo.fomi.hu

14.3 SVPIS

Under contract to the Canadian Space Agency, the University of Calgary has developed a suite of software programs for personal computers to aid potential investigators to formulate technically sound observing proposals. The software enables a potential investigator to explore the impact of a range of observational choices on the scientific goals of the experiment. See Table 13 for what functions the software can perform.

The software will run on IBM PC or compatible computers. Since the graphical, keyboard driven user interface makes extensive use of colour, a colour monitor is recommended (although not essential). The software has been designed to minimise use of system resources, so the software will run on low-end personal computers (albeit slowly). A 386 class computer, or better is recommended. A PostScript driver is included to allow for hardcopy of graphs and simulation results.

The software and user documentation can be obtained on a single floppy disk by contacting A.R. Taylor by e-mail (russ@bear.ras.ucalgary.ca). Alternatively the software can be obtained by anonymous ftp from bear.ras.ucalgary.ca (136.159.55.1). The software is in the outgoing/svlbi directory.

15 VSOP Data Analysis

In general, fringe fitting of VSOP correlated data will be done in the Astronomical Image Processing System (AIPS) and post correlation data analysis will be done in either AIPS or in the Caltech VLBI package. With correlated data from the VSOP correlator coarse fringe fitting, editing and integration can be done at the correlator in a software package called CODA (Correlator Output Data Analyzer). After this the data can be imported into AIPS for further data reduction. However at the request of the PI, the raw correlated data can be written out in a form that can be read directly into AIPS.

15.1 NRAO AIPS

AIPS is a set of programs for the analysis of radio astronomy data, including both continuum and spectral line VLBI data. AIPS is available for a wide range of computer operating systems and several new AIPS tasks have been or are being added to support space VLBI data reduction. Specifically these new tasks include:

1. Single-Baseline Fringe-Fitting. This task is optimized for space VLBI fringe detection. It will allow fringe searching in delay, rate, and acceleration (if required), handle tracking station hand-overs in a graceful fashion, and search for fringes back as well as forward in time, which will be important when apogee occurs before perigee for a given tracking pass.

2. Fringe-Rate Mapping. This task will allow compact sources, for example masers, to be located within an area that is large compared with the synthesized beam. Traditional gridded mapping techniques have difficulty in doing this.

3. Interactive Model-Fitting. For many space VLBI observations, the sparse (u,v) coverage will make model-fitting a desirable data analysis technique. An interactive X-windows interface is being added to AIPS to facilitate this mode of data reduction.

AIPS can be obtained by contacting the AIPS group at aipsmail@nrao.edu. It should be noted that the new space VLBI analysis tasks are implemented in classic AIPS and not in AIPS++. They may be implemented in AIPS++ at a later date.

15.2 Caltech VLBI Analysis Package

An attractive alternative to post fringe fitting data analysis in AIPS is to use the Caltech VLBI package and in particular the program, DIFMAP (Shepherd 1994), which is a mapping and model-fitting package for multi-channel FITS data. DIFMAP can be obtained by anonymous ftp from astro.caltech.ed (131.215.240.1).

16 VSOP Proposal Help

Regional assistance for prospective proposers is available from a number of different sites. Questions relating to the AO, proposal submission, technical aspects of the VSOP mission, or proposal aid software that are not answered elsewhere in this Proposer's Guide or the AO, may addressed via e-mail to these sites. Such questions will also be compiled to create a "Frequently Asked Questions" file, which can be inspected using the World Wide Web (URL: http//www.vsop.isas.ac.jp/), or obtained using anonymous ftp from www.vsop.isas.ac.jp (133.74.2.131). Please refer to this file before contacting the e-mail addresses listed below:

Table 14: E-mail Addresses for Regional Help

Region	e-mail contact
Australasia/Africa	vsop_help@atnf.csiro.au
Canada	vsop_help@ras.ucalgary.ca
Europe/China	vsop_help@nfra.nl
USA	vsop_help@sgra.jpl.nasa.gov
CIS	vsop_help@dpc.asc.rssi.ru
Elsewhere	vsop_help@vsop.isas.ac.jp.

Questions directed to the regional experts will be responded to in a timely manner. As the resources for proposal support are limited, however, questions should be asked as early in the proposal period as possible to avoid any possible congestion during the last weeks before the deadline. These e-mail addresses will be valid until Saturday 18th November 1995.

17 Additional Information

A wide variety of information of additional information on the VSOP mission can be obtained from either the ISAS (URL: http//www.vsop.isas.ac.jp/) or JPL (URL: http//sgra.jpl.nasa.gov/) World Wide Web sites. Proposers should consult these sites to obtain both the latest mission information and to locate references to technical literature describing the mission.

18 Contributors

D. Murphy, P. Edwards, D. Gabuzda, H. Hirabayashi, M. Inoue, H. Kobayashi, D. Meier, G. Moellenbrock, Y. Murata, I. Noszticzius, R. Taylor, J. Ulvestad and A. Wiercigroch provided text, figures or tables for the Proposer's Guide.

19 Acknowledgements

The final version has been improved with comments on earlier drafts from L. Gurvits, R. Linfield, J. Romney, R. Porcas, R. Preston, R. Schilizzi, A. Tzioumis and R. Wietfeldt.

A References

Fujisawa, K. 1995, Ph D Thesis (University of Tokyo).

Hirosawa, H. *et al.* 1994 in "Proceedings of the 19th International Symposium on Space Technology and Science", edited by M. Hinada, Y. Arakawa, Y. Horikawa, J. Kawaguchi, T. Nakajima and I. Nakatani, (Agne Shofu; Tokyo) p. 775.

Levy, G. S., *et al.* 1986, Science, 234, p. 187.

Levy, G. S., *et al.* 1989, Astrophysical Journal, 336, p. 1098.

Linfield, R. P., *et al.* 1989, Astrophysical Journal, 336, p. 1105.

Linfield, R. P., *et al.* 1990, Astrophysical Journal, 358, p. 350.

Linfield, R. P. and Ellis, J. 1994, JPL Interoffice Memorandum # 216 in JPL SVLBI Project Library.

Linfield, R. P. and Kahn, R. D. 1994, JPL Interoffice Memorandum # 179 in JPL SVLBI Project Library.

Moellenbrock, G., *et al.* 1994, in Proceedings of 2nd JIVE/EVN Symposium edited by A. J. Kus, R. T. Schilizzi. K.M. Borowski and L. I. Gurvits, p. 61.

Murphy, D. W. 1994, JPL Interoffice Memorandum # 212 in JPL SVLBI Project Library.

Shepherd, M. C. 1994. BAAS, 26, p. 987.

T. Takano *et al.* 1994 in "Proceedings of the 19th International Symposium on Space Technology and Science", edited by M. Hinada, Y. Arakawa, Y. Horikawa, J. Kawaguchi, T. Nakajima and I. Nakatani, (Agne Shofu; Tokyo) p. 483.

B Acronyms and Abbreviations

α	Right Ascension
δ	Declination
ω	Argument of Perigee
Ω	Right Ascension of the Ascending Node
AIPS	Astronomical Image Processing System
A/D	Analog to Digital
ATCA	Australia Telescope Compact Array
ATNF	Australia Telescope National Facility
AO	Announcement of Opportunity
CIS	Commonwealth of Independent States
DAT	Digital Audio Tape
DSN	Deep Space Network
EVN	European VLBI Network
FITS	Flexible Image Transport System
ftp	file transfer protocol
FWHM	Full Width Half Maximum
GPS	Global Positioning Satellite
GRT	Ground Radio Telescope
GVWG	Global VLBI Working Group
IF	Intermediate Frequency
IRM	Image Rejection Mixer
ISAS	Institute of Space and Astronautical Science
JIVE	Joint Institute for VLBI in Europe
JPL	Jet Propulsion Laboratory
LO	Local Oscillator
LCP	Left Hand Circular Polarization
mas	milli-arcseconds
Mbps	Mega bits per second
NAO	National Astronomical Observatory
NASA	National Aeronautics and Space Administration
NRAO	National Radio Astronomy Observatory
PA	Position Angle
PI	Principal Investigator
QPSK	Quadrature Phase Shift Key
RCP	Right Hand Circular Polarization
RCS	Reaction Control Subsystem
RFI	Radio Frequency Interference
RMS	Root Mean Square
SEFD	System Equivalent Flux Density
SNR	Signal to Noise Ratio
SPAS	Space VLBI Assistance Software
SRC	Scientific Review Committee
SVLBI	Space VLBI
SVPIS	Space VLBI Principal Investigator Software
TDRSS	Tracking and Data Relay Satellite System
URL	Uniform Resource Locator
VLA	Very Large Array
VLBA	Very Long Baseline Array
VLBI	Very Long Baseline Interferometry
VSOG	VSOP Science Operations Group
VSOP	VLBI Space Observatory Programme
WSRT	Westerbork Synthesis Radio Telescope
WWW	World Wide Web

C All-Sky (u,v) Plot Examples

In this appendix are shoen All-Sky (u,v) coverages plotted every three months during AO phase 1 observations with the VSOP spacecraft co-observing with the VLBA. Each (u,v) coverage is for an observation that lasts 4 orbits. Also plotted on these figures are the location of the Sun, the 70° solar avoidance curve, the orbital plane, the orbit normal and orbit anti-normal directions (labeled as N), and the apogee and perigee directions (labeled as A and P respectively).

In order to keep down the size of the Proposer's Guide the examples in the Appendix have been restricted to only one ground array. Proposers are strongly encouraged to obtain the proposal aid software, described in Section 14, to investigate for themselves how the (u,v) coverage varies as a function of the ground array used, epoch of observation and length of observation.